The intrinsic stress of polycrystalline and epitaxial thin metal films

1994 J. Phys.: Condens. Matter 6 9519

(http://iopscience.iop.org/0953-8984/6/45/005)

J. Phys.: Condens. Matter 6 (1994) 9519–9550. Printed in the UK

REVIEW ARTICLE

The intrinsic stress of polycrystalline and epitaxial thin metal films

R Koch

Institut für Experimentalphysik, Freie Universität Berlin, Arnimallee 14, D-14195 Berlin, Germany

Received 18 July 1994, in final form 24 August 1994

Abstract. It is well known that thin films develop large intrinsic stress during their preparation. The intrinsic stress either originates from strained regions within the films (grain boundaries, dislocations, voids, impurities, etc) or at the film/substrate (lattice mismatch, different thermal expansion, etc) and film/vacuum interfaces (surface stress, adsorption, etc) or is due to dynamic processes (recrystallization, interdiffusion, etc). Since the magnitude of most of these stress contributions is directly related to film morphology, important structural information can be extracted from measurements of the intrinsic stress. This article presents a thorough discussion of today's understanding of the growth of thin films and reviews the related atomistic mechanisms responsible for intrinsic stress. On the basis of these ideas recent experimental results on the intrinsic stress of UHV deposited polycrystalline and epitaxial thin metal films are discussed. Depending on the respective growth mode of the films—Volmer–Weber, Stranski–Krastanov and Frank–Van der Merwe modes—characteristic stress behaviours are observed. *In situ* intrinsic stress measurements are therefore a promising new technique to gain additional insight into film growth.

Contents

0953-8984/94/459519+32$19.50

1. Introduction

Thin films have evolved to an important and indeed probably indispensable constituent of modern everyday life. Via VLSI technology (very large-scale integration) they are omnipresent in electronic devices, in particular in all computer systems. Other well known applications concern the refinement of optical devices (lenses, mirrors, filters, etc), solar cells, protection against corrosion and tribology. Regardless of the technique of film preparation (physical or chemical vapour deposition, sputtering, electrochemical deposition, etc) thin films develop large intrinsic stresses in the course of their deposition, which usually asume values that even exceed the tensile strength of the respective bulk phases ($\approx 2 \times 10^8$ *N m*$^{-2}$ *for most metals*). It is therefore not surprising that intrinsic stress is frequently held reponsible for malfunction or failure of technologically important thin-film devices. Worst case scenarios are peeling off or cracking of thin films or altered physical properties. Obviously, from a technological point of view there is a continuous serious interest in measurements of intrinsic stress. The aim of these investigations is to improve the conditions of film preparation in order to fabricate low-stress thin films.

As early as the sixties and seventies considerable effort was spent to relate the intrinsic stress of evaporated thin metal films to respective structural features. For pertinent reviews of this work, particularly of the proposed stress models, the reader is refered to articles by Hoffman [1], Buckel [2], Campbell [3] or Kinosita [4,5]. At that time the vast majority of investigations was performed in high vacuum, where the partial pressures of various residual gas components are still high enough to permit substantial chemical reactivity with the deposited film material (notice that typical high-vacuum partial pressures of 10^{-8} mbar cause one monolayer of contaminants in about 100 s!). However, as the composition of a high vacuum alters from experiment to experiment film growth and thus the related stress development proceeded in an ill defined, hardly reproducible manner. Retrospectively it seems that the final breakthrough for a mechanistic understanding of intrinsic stress was achieved by transfering the stress investigations to UHV. Owing to the well defined low-level vacuum conditions the experimental reproducibility was significantly improved so that it eventually became possible to separate the various parameters of film growth that influence the intrinsic stress of thin films.

Abermann and co-workers investigated simultaneously intrinsic stress and morphology of a large number of different polycrystalline metal films UHV deposited onto amorphous substrates. By varying the growth conditions (substrate temperature [6], partial pressure of

certain components of the residual gas [7–9], deposition rate [10], substrate contamination [11], etc) a stress model, which consistently explains all experimental data, was established. Depending on the mobility of the respective metals two types of stress behaviour were found and correlated with two different modes of island (Volmer–Weber) growth [12], namely columnar grain growth [13–15] and island growth accompanied by additional lateral grain growth in the continuous films [16, 9]. Recently our group—by studying several metal films growing *epitaxially* by Volmer–Weber mode [17–19]—detected another archetypal stress behaviour. To illustrate the three types of Volmer–Weber growth the respective film forces as functions of the mean film thickness of the system Ag/mica(001) are shown in figure 1 (from [17]). Although the detailed discussion is postponed to sections 5 and 6, just a short glimpse of figure 1 impressively demonstrates the power of intrinsic stress measurements: due to the three growth modes three different film force against film thickness curves are observed. Thus, intrinsic stress measurements can be employed as a rapid and inexpensive fingerprint method for film growth studies. Moreover, recent results on thin films growing via Stranski–Krastanov and Frank–Van der Merwe modes indicate that the other two growth modes discussed in literature are also dominated by a very characteristic stress against film thickness dependence [20, 21].

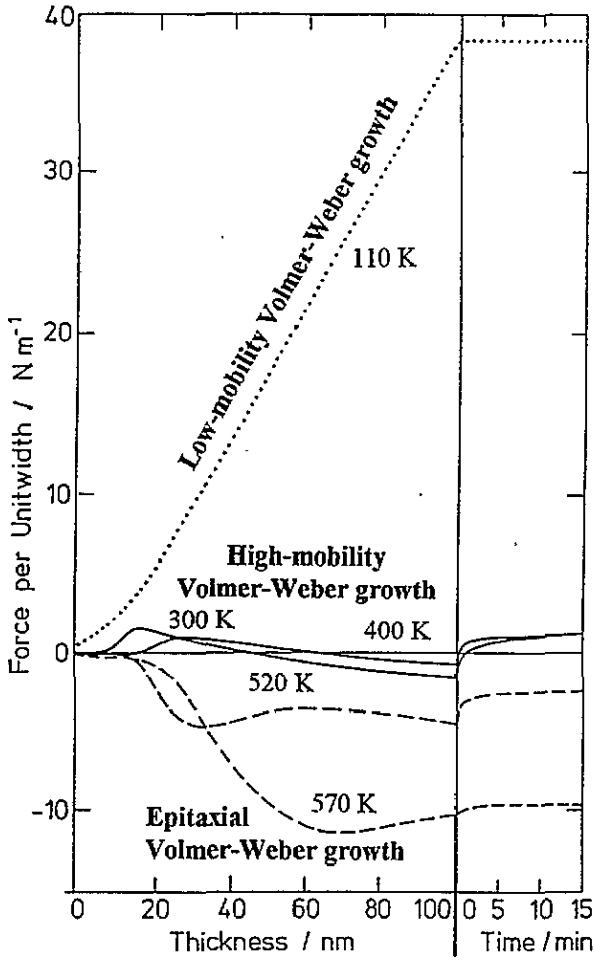

Figure 1. Film forces per unit width against mean thickness (left-hand side) and time (right-hand side) of Ag films UHV deposited onto mica(001) at various substrate temperatures. By convention positive and negative values denote tensile and compressive forces, respectively (from [17]).

In this article recent intrinsic stress measurements (ISMs) on UHV deposited polycrystalline and epitaxial metal films are reviewed with emphasis on a thorough discussion of structural aspects and related stress mechanisms. The article, however, does not cover ISM results for ceramic thin films [22] or for metal films deposited by sputtering techniques (see e.g. [23] or [24]). Section 2 gives a short introduction to the cantilever beam technique, a widely used method for *in situ* stress measurements in UHV. In section 3 the different modes of film growth are discussed including recent developments on the role of kinetic parameters. Section 4 summarizes the most important stress mechanisms. In sections 5 and 6 representative experimental results on polycrystalline and epitaxial metal films, respectively, are presented. The review is concluded by a summarizing discussion in section 7.

2. The measurement of intrinsic stress

The methods most commonly used to study thermal and intrinsic stress of thin films can be divided into two groups: (i) techniques that determine the film stress from the bending of the substrate (beams, plates or discs) and (ii) diffractional methods, which actually measure *strain* such as x-ray diffraction [25, 26] or LEED (low-energy electron diffraction) intensity analysis [27]. For the latter case the film stress is calculated by Hooke's law and therefore requires knowledge of the elastic constants, which are not usually available for thin films. Examples of both classes of techniques have been reviewed in detail in the past (see e.g. [1] or [3]). Here only a brief description of the very common cantilever beam technique is given as it has also been used for the experiments described in sections 5 and 6.

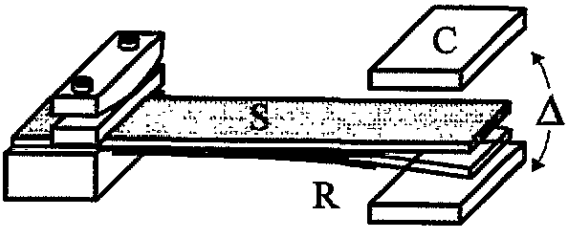

Figure 2. A schematic illustration of the cantilever beam technique for measurement of the intrinsic stress of thin films: the cantilever beam substrate (S) is clamped on its left-hand side, the right-hand end is free to move. One possible means of determining the radius of the substrate curvature (R) is by measuring the respective substrate displacement (Δ) with a differential capacitance technique (C).

A schematic drawing is given in figure 2. The cantilever beam substrate S is clamped on its left-hand side; the other end is free to move when the deposited film is under stress. As long as the film thickness t_f is small compared with the thickness of the substrate t_s, the respective film forces F_f (normalized to unit substrate width $w \equiv w_s = w_f$) are indirectly proportional to the radius of curvature R of the substrate and can be calculated via Stoney's well known formula [28, 29]:

$$F_f/w = \sigma_f t_f = E_s t_s^2/6R. \tag{1}$$

E_s is the appropriate elastic constant of the substrate. Conventionally positive film forces F_f and film stress σ_f are defined to be tensile, i.e. the average lattice parameter of the film

is larger than the equilibrium value $[(a - a_0)/a_0 > 0]$. If, on the other hand, the lattice parameter is smaller one speaks of compressive forces and stress $[(a - a_0)/a_0 < 0]$, which correspondingly are negative in sign.

Polycrystalline or amorphous [30] films deposited onto amorphous substrates such as glass usually exhibit isotropic biaxial stress within the film plane; the elastic constant of equation (1) then is calculated as $E_s = Y_s/(1 - \nu_s)$, with Y_s being Young's modulus and ν_s Poisson's ratio of the substrate [1,31]. In the case of epitaxial films growing on single-crystalline substrates the evaluation of the film forces from the substrate deflection is more sophisticated. In a first approximation the film forces can be estimated by taking Young's modulus Y_s in the crystallographic direction of the long substrate axis. For substrates of the cubic crystal class, e.g., the reciprocal of Young's modulus in direction of the unit vector $r = (r_1, r_2, r_3)$ is calculated from the expression [32]

$$1/Y_s = s_{11} - 2(s_{11} - s_{12} - \tfrac{1}{2}s_{44})(r_1^2 r_2^2 + r_2^2 r_3^2 + r_3^2 r_1^2) \tag{2}$$

with s_{ij} being components of the fourth-rank compliance tensor. Calculation of the exact value of the film forces as well as their correlation with respective film strain ε_{ij}, however, requires detailed knowledge of the epitaxial film structure to solve the tensor equations $\sigma_{ij} = s_{ijkl}\varepsilon_{kl}$ of film and substrate. For uniaxial film stress in the direction of the bending beam axis one obtains $E_s = Y_s$.

The radius of the substrate curvature R can be determined either optically by detecting the change of the reflection angle of a laser beam (see, e.g., [22] or [21]) or—as illustrated in figure 2—by measuring the substrate displacement Δ with capacitance methods (see, e.g., [33], [30] or [34]). In both cases lock-in assisted phase sensitive signal detection guarantees a high sensivity that is even sufficient for stress investigations of films with submonolayer thickness [20, 21] or of adsorbate induced surface stress [35, 34], making ISM an important new technique for surface science studies. Further advantages of the cantilever beam technique are its compatibility with UHV requirements and the fact that it is an *in situ* technique, i.e. the film stress can be measured continuously during the film deposition as well as afterwards in order to study e.g. film recrystallization [36].

3. The nucleation and growth of thin films

The growth of thin films has been studied intensively in the past by employing the entire spectrum of experimental tools ranging from TEM [37], SEM [38], LEEM [39] (transmission, scanning and low-energy electron microscopy), RHEED [40], MEED [41], SPALEED [42] (reflection high-, medium- and spot profile analysis low-energy electron diffraction), AES (Auger electron spectroscopy) [43], and STM (scanning tunnelling microscopy) [44, 45] to He diffraction [46, 47]; in addition, advanced theoretical film growth simulations were performed with high-speed supercomputer systems [48, 49]. It appears, however, that despite these efforts we are still far from a complete understanding of all the processes involved. Nevertheless this section is devoted to a short summary of the present knowledge on nucleation and growth of thin films.

3.1. Thermodynamical considerations

A decisive period of film growth is the nucleation stage at the very beginning of the film deposition. Although thermodynamics as a phenomenological theory is applicable precisely only to macroscopic systems, it may provide useful first insights. Since for the initially

formed nuclei the ratio between the number of surface and/or interface atoms to atoms of the bulk is rather high, their equilibrium shape will depend on the magnitudes of the respective free surface and interface energies. In principle, the size of the crystal facets that contribute to the equilibrium polyhedron can be calculated by extending the ideas leading to Wulff's theorem to heterogeneous nucleation. As a result one obtains a relation [50] between the chemical potential $\Delta\mu$ of the nuclei and the ratio of the free surface energies Φ_i (compare subsection 4.3.1) and the central distance h_i of individual crystal facets (see figure 3(a)):

$$\Phi_i/h_i = (\Phi^* - \Phi_B)/h_{AB} = (\Phi_A - \beta)/h_{AB} = \Delta\mu/2v = (kT/2v)\ln P/P_\infty. \tag{3}$$

Here k, T and v are Boltzmann's constant, the substrate temperature and the volume of a single film atom, respectively; P and P_∞ are the respective vapour pressures of the nuclei and the bulk phase. As illustrated in figure 3(a) the interface is created between surface A of the nuclei and the substrate surface B. The specific free interface energy Φ^* is then calculated as $\Phi^* = \Phi_A + \Phi_B - \beta$ with β being the corresponding free energy of adhesion, which is released when the surfaces A and B are brought into contact. As pointed out by Bauer Φ^* is assumed to be independent of the size and shape of the interface [51]. For an instructive derivation of equation (3) the reader is referred to [52].

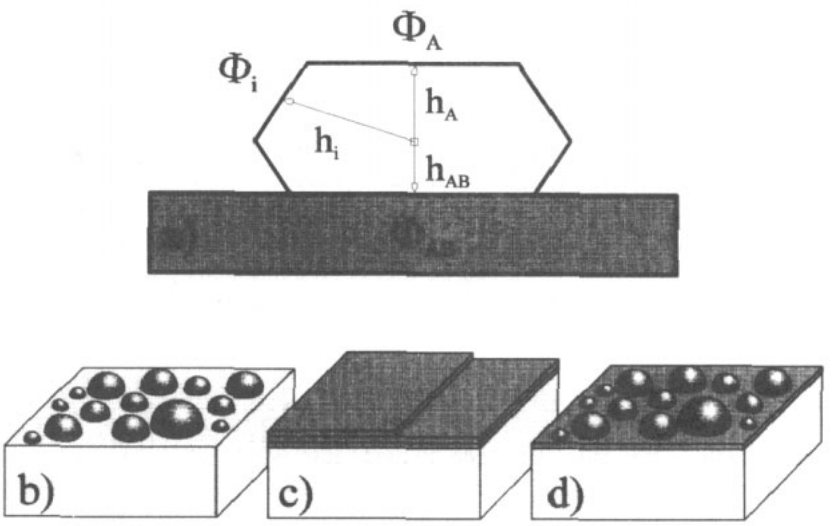

Figure 3. (a) The equilibrium shape of a deposit A on a substrate B; Φ_i and h_i are the free surface energies and central distances of the crystal facets i formed at equilibrium; Φ_{AB} and h_{AB} are the respective values of the interface AB. (b)–(d) A schematic illustration of the three modes of film growth: (b) Volmer–Weber or 3D island mode; (c) Frank–Van der Merwe or layer by layer mode and (d) Stranski–Krastanov mode, where 3D islands nucleate on top of one or a few monolayers.

What can we learn from equation (3) with respect to the growth of thin films? An important clue on the 3D (three-dimensional) shape of the initially formed nuclei is delivered by the central distance of the interface h_{AB}, which in turn is determined by the relative magnitude of the free energy of adhesion β with respect to Φ_A—the free energy of the crystal facet forming the top of the equilibrium nuclei. Depending on the magnitude and the sign of h_{AB} three different modes of film growth can be distinguished.

(i) *Volmer–Weber mode.* In the common case of supersaturation during film deposition ($\Delta\mu > 0$), $h_{AB} > -h_A$ as long as $\beta < 2\Phi_A$. Because the particle thickness t perpendicular to the substrate plane is $t = h_A + h_{AB}$ (compare figure 3(a)) it follows that 3D islands are growing (Volmer–Weber mode: figure 3(b), compare also figure 10). On subsequent growth individual islands coalesce into larger islands that still exhibit equilibrium shapes. For kinetic reasons, however, at some critical island size coalescence into equilibrium shapes is no longer possible [53]. At this stage the first grain boundaries are formed and elongated islands are observed. At percolation, when the films become electrically conducting, the majority of islands grows together (network stage). Upon increasing coverage most of the deposited film material is consumed to fill the remaining open channels (channel stage), i.e. there is no noticable increase in film thickness until eventually the stage of the continuous film is reached. As growth proceeds, depending on the self-diffusion of the film material, the average grain size is preserved (columnar grain growth) or increases laterally due to recrystallization processes.

(ii) *Frank–Van der Merwe mode.* For β approaching $2\Phi_A$ the particle thickness vanishes ($h_{AB} \to -h_A$); this means the films wet the substrate completely and film growth proceeds via the formation of 2D islands in a layer by layer fashion (Frank–Van der Merwe mode: figure 3(c)). This is particularly the case for homoepitaxial systems where $\beta = 2\Phi_A$. Notice, however, that basically the same growth stages as for the 3D Volmer–Weber mode—network stage, channel stage, continuous layer—are passed, although in 2D.

(iii) *Stranski–Krastanov mode.* Frequently a third growth mode is observed in thin-film investigations, where 3D islands start to grow on top of one or a few monolayers (Stranski–Krastanov mode: figure 3(d)). The reason for this more complex growth behaviour lies in the specific nature of the interfaces formed. Obviously the free surface energy of the first deposited monolayers still deviates significantly from the value Φ_A of the film material, possibly due to intrinsic stress (e.g. misfit stress [54]) or due to the formation of an interface alloy or compound. The interface layer therefore can be regarded as a new substrate, for which the thermodynamical considerations above become effective again.

Unfortunately two major obstacles are encountered upon applying the rather plausible thermodynamical theory to real film/substrate systems: (i) to date there is still an enormous lack of experimental data on the free surface and interface energies for the numerous possible combinations of metal and substrate surfaces, so that the predictional value of thermodynamics for the growth of thin films remains poor and (ii) usually film growth does not proceed in thermodynamical equilibrium but is controlled by kinetic parameters as well.

3.2. The role of kinetic parameters

The idealized thermodynamical picture discussed above relies on the assumption of a homogeneous substrate surface, which is characterized by a uniform Φ^* over large distances. In practice, however, such surfaces are hardly ever available. Real substrate surfaces usually exhibit many different defects such as vacancies, adatoms, step and kink sites [55], stacking faults [56], dislocations [57], domain boundaries if the substrate surface reconstructs [58] and impurity atoms or molecules, which have either diffused out of the bulk or adsorbed from the residual gas. As a consequence of the inhomogeneous Φ^*, nuclei of various equilibrium shapes are formed at the initial stages of film growth. In addition, most of these defects can be regarded as energetic sinks for diffusing atoms, as they provide adsorption sites, where the number of nearest neighbour atoms is increased compared with sites on the flat surface. Due to the resulting stronger bonding the mean residence time of diffusing atoms at such defect sites is significantly increased and thus also the chance of combining with other

atoms to form a supercritical nucleus. The presence of defects on surfaces therefore may have substantial influence on the nucleation rate leading to a drastically increased density of nuclei (e.g. decoration of steps [59]). In the same way, defects usually effect strongly diffusion controlled processes of the growing films.

A parameter that counteracts the influence of defects on the kinetics of film growth is the substrate temperature, which determines the thermal energy of the diffusing atoms. Several studies [46,47,60,61] performed recently on conceptually simple homoepitaxial systems revealed very clearly the interaction between defect density and substrate temperature. Although 2D layer by layer growth is undoubtedly demanded by thermodynamics, remarkable deviations were observed depending on the substrate temperature, indicating that the influence of certain types of defect is gradually overcome when the substrate temperature is raised.

As long as the temperature is high enough, the diffusion length of the atoms suffices to reach the nearby ledges of steps, which are always present on real surfaces. The arriving atoms are then predominantly absorbed by the steps and film growth proceeds via a continuous movement of the step edges of existing terraces along the substrate surface. This growth mechanism is therefore also known as step flow growth [62]. At slightly lower temperatures, when the mean free path of the film atoms falls beyond the average terrace width, 2D islands nucleate on the terraces. They increase in size during further growth until they percolate. Nucleation of the next layer does not set in until nearly all channels of the preceding layer are filled. As the step density during this type of layer by layer growth alternates between high and low values, it gives rise to the well known intensity oscillations of RHEED [40], MEED [41] and He diffraction [46]. An impressive visualization of this growth mode with STM was recently reported by Stroscio *et al* [61]. At even lower temperatures 3D growth suddenly sets in. As discussed by Kunkel *et al* [46] the thermal energy of the atoms impinging on extended 2D islands now no longer suffices to surmount the diffusion barrier built up by the step edges [63]. As a result, new 2D islands nucleate on existing 2D islands, which altogether leads to 3D growth. On further reduction of the substrate temperature, surprisingly, 'reentrant' 2D growth is observed again [46]. Due to the low substrate temperature the nucleation density of the growing films is now rather high, the size of the 3D islands correpondingly small. It seems that the barrier for downward diffusion of the rougher edges of small islands is considerably lower so that it is overcome again. A dramatic change in film morphology is observed, when the diffusion along the step edges becomes the rate limiting process of film growth. In this case all particles that arrive at step edges stick. The morphology of the growing films then assumes dendritic shapes of fractal geometry in agreement with theoretical predictions [64] for diffusion limited aggregation (hit and stick mechanism). Dentritic growth was observed with STM for Ag/Ag(111) at 100 K [65] as well as for Au/Ru(111) at room temperature [66].

The results obtained so far on the homoepitaxial systems provide already a very comprehensive picture of the role of defects for the growth of thin films, although admittedly the systems investigated are very 'ideal' compared with films of technological relevance. More realistic film/substrate systems usually exhibit several other types of imperfection, which determine and influence the morphology of the growing films. Polycrystalline films, e.g., inherently contain many small-angle grain boundaries, which separate the randomly oriented single-crystalline grains. Heteroepitaxially grown films, on the other hand, usually generate misfit dislocations to account for the misfit stress due to the different lattice parameters of film and substrate. Another problem concerns alloying at the interface layer [67]. For Au/Ni(110) intermixing in the first layer was observed, although it is forbidden for the bulk phases from the 3D phase diagram [68], which implies that the possibility of

alloying actually has to be checked for each particular system. In recent studies small amounts of adsorbates (e.g. O [69] or Sb [70]) that continuously float out to the surface of the growing film have also been employed as 'surfactants' to enhance the degree of epitaxy of thin films. All in all, the situation is much more complex for heterogeneous film/substrate systems. Nevertheless, the nucleation stage can still be regarded as the most important period of film growth as here the morphology of the films at the end of the coalescence stage, when they become continuous, is established. However, if the films are continuous, further growth proceeds quasihomogeneously on their own substrates where essentially the conclusions derived from the homoepitaxial systems apply.

4. Mechanisms of intrinsic stress

Ideally, thin films are free of stress. They have grown epitaxially to *perfect* single crystals onto substrates with identical lattice parameters, hopefully at the temperature of their future application. So far, however, such films only have virtual existence in the dreams of the manufacturers. As discussed in detail in the preceding section, in reality film growth by no means proceeds in thermodynamical equilibrium, most of the growth processes are predominantly kinetically controlled. Therefore thin films in general contain many defects of different types, which constitute departures from the ideal crystal structure and thus may act as sources of stress. In this section the most common stress contributions are discussed and classified according to their range of action—either within the films or at the film/substrate and film/vacuum interfaces.

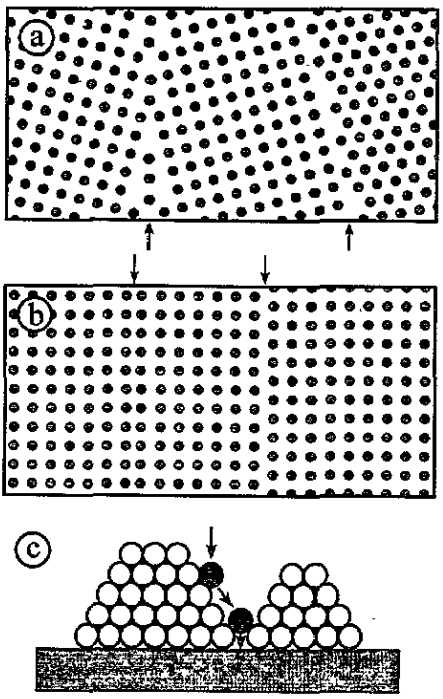

Figure 4. A schematic illustration of examples of grain boundaries separating single-crystalline grains: (a) small-angle grain boundaries of polycrystalline thin films and (b) domain walls separating epitaxially oriented islands of epitaxial thin films. (c) A schematic illustration of the process of domain wall formation in the course of which compressive stress is generated (see the text).

4.1. Stress contributions within the films

4.1.1. Small-angle grain boundaries. Polycrystalline films, in particular those growing by columnar grains, naturally exhibit a high concentration of small-angle grain boundaries, which separate the randomly oriented grains. A schematic illustration is shown in figure 4(a), where the boundaries between the three crystallites are easily recognized as regions of reduced density. Grain boundaries have been presumed from very early on to be a possible source of intrinsic stress. According to Hoffman '... the interatomic forces at the boundaries tend to close any existing gap, with the result that the neighbouring crystallites are strained in tension' [1]. The resulting tensile stress σ_{gb} is proportional to the total grain boundary area and therefore depends inversely on the average grain size $\overline{D}$, i.e. it is larger for finer-grained films:

$$\sigma_{gb} = \frac{E_s}{1-\nu_s}\frac{\overline{d}}{\overline{D}}. \tag{4}$$

$\overline{d}$ is the 'average atomic relaxation distance' at small-angle grain boundaries [1]. Notice, however, that not all grain boundaries necessarily have to be strained. For example, the interatomic forces at equilibrium grain boundaries cancel out—a problem readily programmed in computer simulations [71]. In real films, however, nucleation of the later grains and in particular their positions relative to each other are controlled by the substrate. Usually, when the grains grow together, they are not located in the correct position to form equilibrium grain boundaries. The unanimous result of all investigations performed so far on the numerous polycrystalline thin-film systems is that small-angle grain boundaries on average produce a tensile stress contribution in the films (see, e.g., [72], [73] or [74]). Grain boundary stress may also serve as explanation for the large tensile stress observed in amorphous metal films [30]. As has been shown by the high-resolution TEM investigations of Zweck *et al* [75,76] amorphous alloys consist of well ordered regions with dimensions of 2–4 nm, which can be regarded as randomly oriented nanocrystallites.

4.1.2. Domain walls. In the case of epitaxial growth, when epitaxially oriented islands coalesce, a special type of grain boundary may be formed. An example is provided by epitaxial Volmer–Weber systems. Here intrinsic stress measurements [20] revealed that due to the weak film/substrate interaction no stress component due to the misfit between the different lattice parameters of film and substrate is generated. Isolated islands therefore grow free from stress with the lattice parameter appropriate for the film material. However, since they have nucleated at positions determined by the substrate, the lattices of the coalescing islands may be improperly spaced either along one or along two dimensions as illustrated in figure 4(b). The boundaries between different islands can be regarded also as domain walls, because they separate epitaxial film domains. Respective stress investigations so far have revealed that on average compressive stress develops at domain walls [20], a result that is in contrast to the tensile stress of small-angle grain boundaries. Atoms that arrive at the domain walls and close the gap between formerly isolated islands can form a larger number of energetically favourable nearest-neighbour bonds by immersing in the respective deepest layer (figure 4(c)) and thereby generating compressive strain in both epitaxial islands. This interpretation is supported by the magnitude of the strain energy determined experimentally during domain wall formation (figure 15); this is of the order of about one metal–metal bond [19] and therefore certainly smaller than the respective gain in bonding energy.

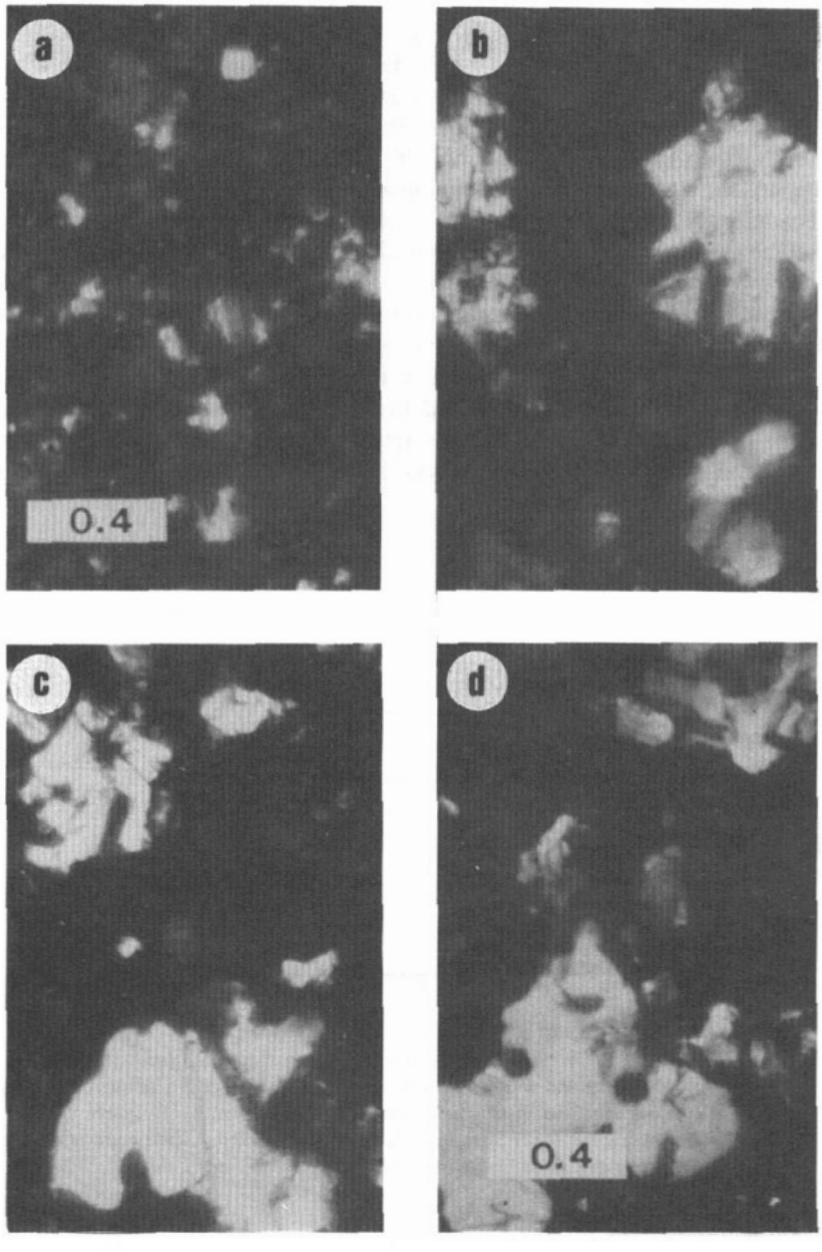

Figure 5. Transmission electron micrographs of 100 nm thick Au films: (a)–(c) Au films coated with 10 nm MgF_2 and exposed to air 30 min after deposition, micrographs taken 1 h, 3 h and 20 h after the metal deposition, respectively; (d) a bare Au film, micrograph taken 1 h after the metal deposition; the scale bar is in micrometres (from [36]).

4.1.3. Recrystallization processes. If the self-diffusion of the deposited film material is high enough, the films may recrystallize actually during the film deposition and also after the completion of the deposition. In the course of such processes defects are annealed and the

average grain size of polycrystalline films is increased. The TEM images of figure 5 serve to illustrate film recrystallization [36]. Figures 5(a)–(c) document the ongoing restructuring of a 100 nm thick polycrystalline Au film that has been coated immediately after its deposition in UHV with a 10 nm thick MgF_2 film. Despite the protective layer the average grain size increases continuously with time until after about 20 h a stable configuration is achieved. The film then exhibits many grains with lateral dimensions of several micrometres. For comparison, a TEM image of an analogously prepared bare Au film, taken 1 h after film preparation, is depicted in figure 5(d). Surprisingly the morphology of the bare film closely resembles that of the protected film after 20 h (figure 5(c)). Moreover, no noticeable changes in average grain size are observed when investigating the bare film after longer periods of time, indicating that both films approach the same equilibrium configuration. Since both films were prepared simultaneously, i.e. at the same preparation conditions, they exhibited identical morphology at the end of film deposition. However, the time necessary to reach the stable configuration characterized by grains in the micrometre range is much larger for the protected film. Obviously the rate of recrystallization is considerably reduced by coating thin films with protective layers, although one has to be aware that restructuring is not totally inhibited.

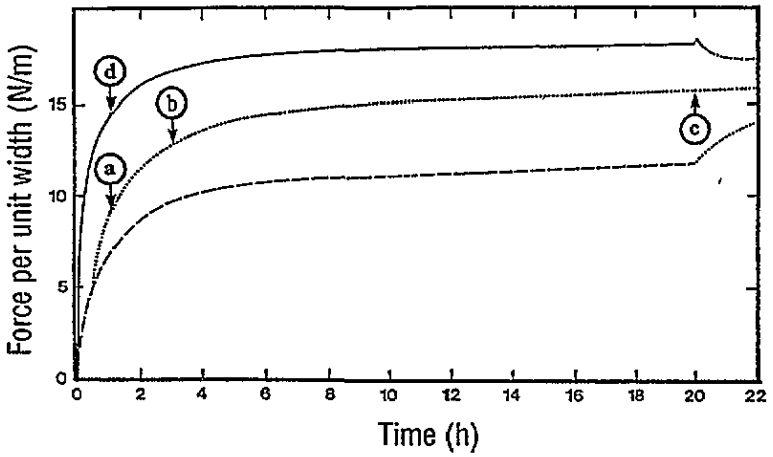

Figure 6. The change of the film forces after the deposition of 100 nm thick Au films without (solid line) and with a 10 nm thick coating layer of MgF_2 (dashed line) as a function of time in vacuum, and in laboratory atmosphere (dotted line). The force changes occurring due to exposing the MgF_2 layer to air have been subtracted. Labels correspond to the respective TEM micrographs of figure 5 (from [36]).

By eliminating all kinds of defect (grain boundaries, voids, point defects, etc), recrystallization processes usually lead to a densification of the films and therefore should give rise to a tensile stress contribution (see below). The structural changes of the Au films from above can indeed be correlated with the simultaneous development of tensile stress. Figure 6 shows the corresponding film forces measured as a function of time after the deposition of both films [36]. The film forces of the bare film reach about 85% of their final value ($\approx$ 17 N m^{-1}) within 1 h, while the force changes of the protected film are considerably smaller in the same period of time (38%). Moreover, as long as the protected film it is kept in UHV only two thirds of the total film forces are generated. However, upon exposing the

protected film to laboratory air—a necessary procedure for common TEM investigations—an accelerated force development is observed in the course of which about 90% of the respective forces of the bare film are generated after 20 h. Diffusion of laboratory air into the MgF_2 layer (as indicated by respective force changes, for details see [36]) probably weakens its capability to prevent recrystallization in the Au film underneath. All in all the temporal dependence of the film forces directly reflects the amount of recrystallization leading to the morphologies imaged by TEM (figure 5).

Chaudhari [77] tried to quantify the stress contribution due to recrystallization processes by assuming a volume Δv_{ex} present in excess per unit area of grain boundaries compared with the perfect single crystal. By elimination of grain boundary area during grain growth from an initial average diameter D_0 to a final value of D the following biaxial stress σ_{recr} develops:

$$\sigma_{recr} = \frac{2E}{1-\nu}\Delta v_{ex}\left(\frac{1}{D_0} - \frac{1}{D}\right). \tag{5}$$

Using the data on morphology and stress of figures 5 and 6 a reasonable value for Δv_{ex} of about 0.1 nm is obtained. Notice, however, that in calculating the σ_{recr} by equation (5) no additional stress contributions have been considered that account for the elimination of strained regions in the films due to recrystallization, which would reduce or increase the recrystallization stress depending on the sign of strain, tensile (e.g. at non-equilibrium small-angle grain boundaries, subsection 4.1.1) or compressive (e.g. due to capillarity stress, subsection 4.1.5). Recently Chaudhari's procedure has been extended by Doerner and Nix [78] to derive an expression for the respective rate of stress generation as well as to calculate the stress development during annealing of vacancies and voids in thin films.

4.1.4. The lattice expansion mechanism. As outlined in detail in subsection 3.1 the free surface and interface energies play an important role in determining the mode of film growth. Here another aspect of surfaces and interfaces is discussed, which concerns their influence on the equilibrium lattice parameter of small particles. Meanwhile it is well established that due to capillarity effects the lattice parameter of isolated metal particles of radius R is smaller than that of the respective bulk phase [79–81]. As the particles grow, their equilibrium lattice parameter $a(R)$ increases and gradually approaches the respective bulk value a_0. In the case of thin-film growth, however, accommodation to the respective equilibrium value $a(R)$ may be inhibited, because the particles are anchored to the substrate by adhesion. According to a stress model by Finegan and Hoffman [82], due to the expansion of the crystal lattice upon particle growth a compressive strain develops inside the particles, which should show up as compressive stress contribution during the island stage of film growth.

Assuming liquid like particles with a uniform surface tension Φ, the magnitude of the corresponding compressive stress can be estimated by means of the Laplace equation, which relates the pressure P inside small droplets to their radius R [83]:

$$P = -2\Phi/R. \tag{6}$$

With $P = K(\Delta V/V_0) \approx 3K(\Delta a/a_0)$ the lattice parameter $a(r)$ as function of its distance r from the particle centre is calculated as $a(r) = a_0[1 - 2\Phi/(3Kr)]$; K and V are the bulk modulus and volume of the particles, respectively. Obviously the interior atomic distances are compressed when compared with the equilibrium parameter $a(R) = a_0[1 - 2\Phi/(3KR)]$ that corresponds to particles of diameter R. For a growth model consisting of hemispherical

particles of uniform size (figure 7, section 5) the film forces (normalized to unit substrate width w) that accumulate until percolation due to the lattice expansion mechanism are of the order of Φ, which usually exhibits values of a few newtons per metre [84]. ISMs performed so far on various polycrystalline and epitaxial Volmer–Weber films, however, revealed no film forces of that size at the initial growth stages (see sections 5 and 6). It seems that due to the weak film/substrate interaction adhesion of the particles is not strong enough to withstand the compressive stress so the majority of the lattice expansion strain is continuously relaxed upon particle growth. Notice, however, that lateral strain relaxation via particle gliding is no longer possible at percolation, when the previously isloated particles touch and a coherent network is formed. As a consequence a strain field corresponding to the particle radius R_p at percolation is stored in the films. As will be discussed in the next paragraph this strain field gives rise to a compressive stress contribution in the continuous films.

4.1.5. The capillarity stress. As discussed in subsection 4.1.4 due to capillarity effects the lattice parameter of isolated 3D metal particles is smaller than in the bulk. Upon particle growth, gliding at the interface usually ensures that the atomic distances are adjusted to the respective equilibrium value. Strain relaxation by gliding, however, is no longer possible at percolation, when the majority of particles touch to form a coherent network. As a consequence a strain field is stored in the film, which directly reflects the average particle radius R_p at percolation. For $R_p > 10$ nm the 'capillarity strain'—calculated by equation (6)—is less than 0.1%, which for comparison is at least one order of magnitude smaller than ordinary values of lattice misfit. According to Abermann *et al* [10] the capillarity strain is propagated into the growing film after the remaining open channels have been filled and therefore gives rise to a respective compressive stress contribution in the continuous film ('capillarity stress'). Depending on the deposition conditions the capillarity stress may be observed up to film thicknesses of several hundred nanometres until the information of the strain field is eventually lost due to the formation of defects or due to the incorporation of molecules from the residual gas atmosphere into the film.

4.1.6. Impurities. It is well known that growth and morphology of thin films are strongly influenced by the vacuum conditions during the film deposition. More precisely, the determining factor is the relative impingement rate i^*, i.e. the ratio between the deposition rate r_d (monolayers per second) and the impingement rate i (monolayers per second) of a certain component of the residual gas with partial pressure P_d (Torr). For sticking coefficients close to unity i^* ($\equiv r/i \approx 10^{-6} r_d/P_d$) should exhibit values of at least 100–1000 to ensure 'clean' deposition conditions. Recent ISM studies have shown that deposition of more reactive metals such as Cr [14], Fe [15, 74] or Al [9] at elevated O_2 partial pressures leads to the formation of oxide films, when the relative impingment rate approximately resembles the composition of the oxides. At lower partial pressures O is incorporated into the films probably at interstitial sites or at grain boundaries as can be concluded from the corresponding compressive stress contribution. An analogous behaviour was observed for Al films evaporated at H_2O partial pressures up to 1×10^{-5} mbar [9]. Less reactive metals such as Ag or Cu are not oxidized up to partial pressures of 10^{-5} mbar, but a considerable enhancement of the nucleation rate is observed due to the decreased surface diffusivity [8]. Chemical reaction with residual gas, however, is not restricted to O_2 and H_2O, which are commonly agreed to be quite reactive components. Deposition of Ti in an otherwise inert N_2 atmosphere, e.g., leads to the formation of TiN [85].

4.2. Stress contributions in the film/substrate interface

4.2.1. Misfit stress. In the case of epitaxial (= oriented) film growth the lattices of film and substrate are not usually identical but differ at least with respect to the magnitude of the lattice constants in certain crystallographic directions. For thin films deposited onto thick substrates the misfit f (along a certain crystallographic direction) is conveniently defined as

$$f = \frac{a_s^0 - a_f^0}{a_s^0} \tag{7}$$

with a_f^0 and a_s^0 being the stress free lattice constants of film and substrate, respectively. If the misfit does not exceed a critical value f_{crit}, which is usually of the order of several per cent, at least the first film layers may grow pseudomorphically, i.e. with perfect registry between film and substrate atoms. In this growth stage the misfit is completely accomodated by elastically straining of the films, which means that simultaneously a respective misfit stress contribution should be observed. It is noteworthy that the misfit stress—depending on the magnitude of the misfit—can assume values of 10^9–10^{10} N m^{-2}, which are huge compared with the contributions of other stress mechanisms [20]. The strain energy $U_{mf} = E_f \varepsilon^2 t_f$ due to the misfit increases linearly with film thickness t_f; for coherent growth the elastic strain ε is equal to f, for isotropic biaxial misfit the elastic constant E_f is $Y_f/(1 - \nu_f)$. As growth proceeds eventually a critical film thickness t_{crit} is reached where it becomes energetically more favourable to introduce misfit dislocations for total or partial strain relief. In the past decades considerable effort was spent to theoretically predict the values of f_{crit} and t_{crit}. The main difficulty arises in calculating the energy U_{md} per unit length of the misfit dislocations; notice that U_{md} includes both the energy of disregistry and the energy of the localized strain at the misfit dislocation. The two analytical approaches used frequently are based either on the Frenkel–Kontorowa model [86, 87] or on the Volterra continuum model for edge dislocations [88, 90]. Both models yield fair agreement with experiment, but due to the simplifying assumptions the theoretical values for f_{crit} and t_{crit} are generally significantly lower than the experimental ones. For in-depth reviews on this issue the reader is referred to articles by Matthews [89, 90] and Van der Merwe and Jesser [91].

4.2.2. Solid state reactions and/or interdiffusion. When two solid phases—in our case the substrate S and a metallic film F—are brought together, they may undergo a chemical reaction, by means of which a new compound (alloy for metallic substrates) F_pS_q is formed at the interface. Useful information on possible chemical reactions are provided by the respective 3D phase diagrams. Frequently solid state reactions are accompanied by considerable stress generation. As emphasized by Zhang and d'Heurle [92], however, the magnitude and sign of the stresses cannot not simply be derived from comparing the volumes of the educts ($pF + qS$) and products (F_pS_q) of the chemical reaction. Once a continuous layer of F_pS_q has formed, which separates the two solid phases F and S, the rate of reaction is additionally determined by the diffusion of species F and S in the intermediate layer. If one species is more mobile than the other, the new phase will predominantly grow at the interface lying opposite to the faster component. Therefore only the volume of the less mobile phase has to be considered, which explains e.g. the appearance of compressive stress during the formation of $PtSi_2$ or $PdSi_2$ [93]. In the latter case the overall stress behaviour, however, is even more complex, as the reaction stress is superimposed by relaxation effects.

A further stress contribution may arise from mobile species, which are incorporated into the substrate and diffuse into the growing film. Abermann [94] studied the intrinsic

stress of clean Al films evaporated onto Al substrate films, which were deposited at elevated O_2 partial pressures and therefore contained a considerable amount of dissolved O. Here migration of O into the clean films leads to a tensile stress contribution. Winau *et al* [95], on the other hand, observed a compressive stress contribution upon interdiffusion of O from superconducting $YBa_2Cu_3O_{7-x}$ substrate films into Ag and Au films above 570 K, indicating that different mechanisms control the development of stress in the two examples.

4.2.3. Thermal stress. In contrast to the stress mechanisms discussed so far thermal stress σ_{th} is an extrinsic stress. It is not the result of the growth process but usually arises when the external parameter 'temperature' (T) is changed after the film deposition. Thermal stress originates in the different thermal expansion coefficients of film (α_f) and substrate (α_s), which causes a thermal strain ε_{th} to be built up in the film:

$$\sigma_{th} = \frac{E_f}{1-\nu_f}\varepsilon_{th} = \frac{E_f}{1-\nu_f}\int_{T_0}^{T}(\alpha_f - \alpha_s)\,dT. \tag{8}$$

As discussed in detail by Murakami [96] the thermal stress calculated by equation (8) is observed only over a limited temperature range (elastic region). When the thermal strains exceed the elastic limit of the film, they are relaxed by various mechanisms such as dislocation glide or grain boundary diffusional creep. As the relaxation processes are inherently accompanied by simultaneous changes of the film morphology they are often detrimental for the stability and performance of thin-film devices, which are not operated at their fabrication temperature.

4.3. Stress contributions in the film/vacuum interface

4.3.1. Surface stress. Due to the reduced number of bondings at surfaces, the equilibrium interatomic distances of isolated surface layers are usually different from that of the bulk. Consequently, if the surface layers are arranged coherently with the crystal planes beneath, they experience stress, precisely surface stress. The physical property 'surface stress' straightforwardly arises by extending the thermodynamical concept of the 'surface tension', which was introduced to describe the surfaces of liquids, to the solid state. Originally the surface tension γ is Gibbs' free energy (i.e. the reversible work) necessary for creating a unit area of liquid surface (A): $\gamma = (\partial G/\partial A)_{P,T,n}$. The free surface energy γ of solids is defined in analogous manner provided that the atomic density of the solid surfaces—as in the liquid case—remains unchanged during expansion. Creation of new surface at constant atomic density, however, is only one of two possibilities for solids. New surface is also obtained by elastically stretching a pre-existing surface, i.e. by lowering the respective surface density. According to Shuttleworth [97] the corresponding free energy due to the elastic deformation of surfaces can be calculated by means of the surface stress tensor g_{ij}, which is the strain derivative per unit area of the energy needed to create the respective surfaces (γA):

$$g_{ij} = (1/A)\partial(\gamma A)/\partial\varepsilon_{ij} = \gamma\delta_{ij} + \partial\gamma/\partial\varepsilon_{ij}. \tag{9}$$

δ_{ij} is the Kronecker delta. While γ, analogous the surface tension of liquids, is a positive scalar and therefore independent of direction, g_{ij} due to the term $\partial\gamma/\partial\varepsilon_{ij}$ is a second-rank tensor. $\partial\gamma/\partial\varepsilon_{ij}$ accounts for the change of γ upon straining the surface in certain directions and may assume positive (tensile) or negative (compressive) sign. An good introduction into the field of surface and interface stresses can be found in [98]. It should be mentioned

that the free surface energies Φ_i used for deriving equation (3) included both the energy of formation and that of possible strains.

Several first-principles calculations performed in the last few years revealed that it is more the rule rather than the exception that single-crystal surfaces are subject to surface stress. As found e.g. for Al(111) and Al(110) [99], $\partial\gamma/\partial\varepsilon_{ij}$ is of the same order of magnitude as γ itself, namely about 1 N m^{-1}, which means that g_{ij} too can be positive or negative (compare equation (9)). If the surface stress is high enough, the chemical bonds to the second layer may be broken in order to develop more stable reconstructed surface configurations. For the unreconstruced (001) surfaces of Ir, Pt and Au, e.g., a large tensile stress was identified as the driving mechanism for the formation of the well known quasihexagonal overlayers [100]. For the unreconstructed surface of Si(111), on the other hand, only a weak compressive stress was calculated [101], indicating that the (7×7) reconstruction is not induced by surface stress.

So far no absolute measurements of surface stress are available [102]. In a number of recent experiments, however, the difference in surface stress due to the adsorption of a monolayer of metal or gas atoms has been measured. Upon formation of the $(\sqrt{3}\times\sqrt{3})R30°$ superstructure of Ga on Si(111)(7×7) a surface stress difference of 1.3 N m^{-1} was determined. The surface stress observed during deposition of Ge [103] and Ag overlayers [19] onto Si(001)(1×2) is equal to the stress resulting from the misfit between the film and substrate lattices. Sander and Ibach [104] investigated the adsorption of O on Si(111)(7×7) and Si(001)(1×2). Whereas one monolayer of O causes a large compressive stress change of -7.2 N m^{-1} on Si(111), a tensile stress change of $+0.26$ N m^{-1} was observed on Si(001), both values in reasonable agreement with cluster calculations based on a valence bond model. High values of adsorbate induced surface stress changes (-6–8 N m^{-1}) were also found for 0.5 monolayers of O, C and S on Ni(001) [105].

5. The intrinsic stress of polycrystalline thin films

The majority of stress investigations perfomed so far deals with polycrystalline metal films deposited onto polycrystalline or amorphous substrates (glass, coated glass, etc). Due to the weak film/substrate interaction film growth proceeds by Volmer–Weber mode, i.e. 3D islands nucleate at the initial stages of film growth (see subsection 3.1). As no preferred directions are imposed by the substrate, initial islands as well as the later grains of the continuous films have random orientations, both within the substrate plane and azimuthally. It is well known that the nucleus density at the very beginning of film growth as well as the average grain size of thicker films is strongly influenced by the mobility of the film atoms, which as a rule of thumb is lower for a higher melting point of the film material. From metals with melting points higher than about 1800 K finely grained films are obtained upon room temperature deposition ($T/T_m < 0.2$). The average grain size of such films is approximately 10 nm and does not vary with film thickness. Since the grains of such films therefore exhibit columnar shapes, one speaks also of columnar grain growth. Metals with lower melting points, on the other hand, are more mobile; this concerns both the surface and the self-diffusion of the film atoms. The density of nuclei formed at the beginning of film growth therefore is significantly smaller than for columnar grain films. As illustrated in figure 7 consequently the average island at percolation and the later grain size are increased. Moreover in the continuous films the self-diffusion is sufficient to permit considerable recrystallization, which manifests itself in additional lateral grain growth (compare also figure 10). Depending on the mobility of the film material, i.e. depending on the respective type of Volmer–Weber

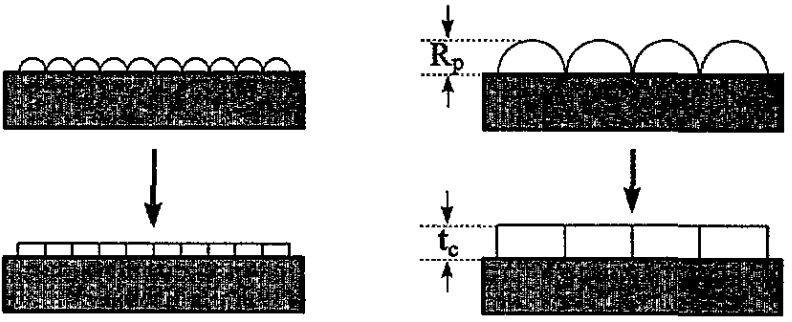

Figure 7. A schematic illustration of the relation between the density of nuclei and the island radius R_p at percolation as well as the average grain diameter $\overline{D}_c$ at the film thickness t_c, where the film becomes continuous. Notice that, for a simple growth model based on the assumption that after percolation at first all open channels are filled, $\overline{D}_c = 2R_p = 2t_c$.

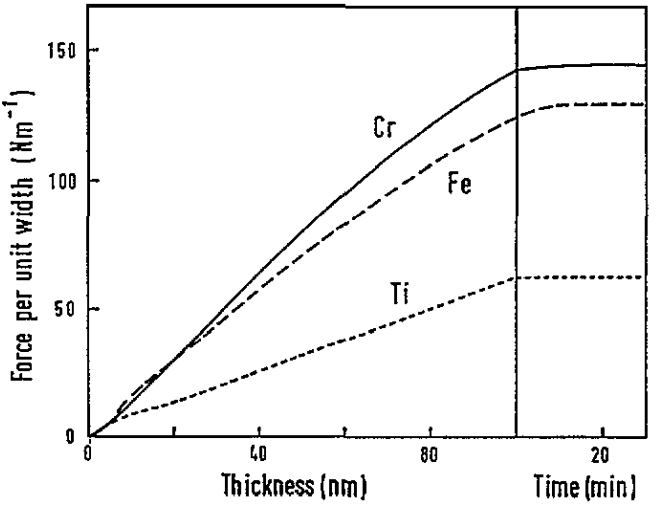

Figure 8. Low-mobility Volmer–Weber growth: film forces per unit width against mean thickness (left-hand side) and time (right-hand side) of Fe, Cr (from [15] by courtesy of R Abermann) and Ti films (from [6] by courtesy of R Abermann) UHV deposited at room temperature onto MgF_2 coated glass substrates.

growth (low-mobility or high-mobility Volmer–Weber growth) two different types of stress behaviour are observed, which will be discussed in the following.

5.1. Low-mobility Volmer–Weber growth (columnar grain growth)

Polycrystalline films of metals with higher melting points ($T/T_m < 0.2$), which grow via columnar grains at room temperature, exhibit a very simple stress behaviour. As examples the film forces of Cr, Fe (from [15]) and Ti (from [6]) films are shown in figure 8. The film forces are tensile and increase nearly linearly with film thickness, indicating a constant film stress independent of film thickness with values of 1.4×10^9 N m^{-2} for Cr, 1.3×10^9 N m^{-2} for Fe and 0.6×10^9 N m^{-2} for Ti. Analogous stress behaviour was determined previously by Klokholm and Berry for many other high-melting-point metals

deposited at high-vacuum conditions [106]. In the case of low-mobility Volmer–Weber growth the intrinsic stress is dominated by the tensile stress at the grain boundaries (see subsection 4.1.1), which constitute the main defects in columnar grain films. As, due to the absence of recrystallization processes, the grain size is nearly independent of film thickness, the total grain boundary area increases almost linearly with film thickness and thus the corresponding film forces. Notice also that there are only very small changes of the film forces after the film deposition has been finished; these are probably due to minute thermal effects (subsection 4.2.3). This confirms that due to the low mobility of the films recrystallization processes (subsection 4.1.3) are indeed frozen in for Cr, Fe and Ti.

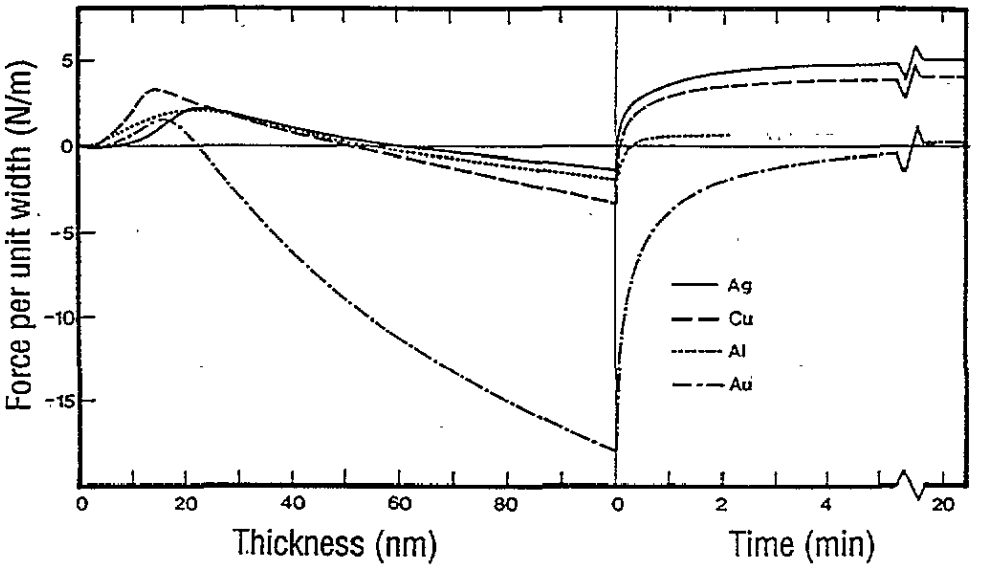

Figure 9. High-mobility Volmer–Weber growth: film forces per unit width against mean thickness (left-hand side) and time (right-hand side) of Ag, Cu, Au (from [16]) and Al films (from [9] by courtesy of R Abermann) UHV deposited at room temperature onto MgF_2 coated glass substrates.

5.2. High-mobility Volmer–Weber growth

Figure 9 shows the film forces of the low-melting-point metals Ag, Cu, Au (from [16]) and Al (from [9]), which were evaporated at room temperature onto MgF_2 coated glass substrates. Obviously the dependence of the film forces on film thickness differs in several points from that of the high-melting-point metals discussed in the previous section: (i) The film forces are at least one order of magnitude smaller than that of the columnar grain films. (ii) The film forces are tensile and compressive as well. (iii) After finishing the film deposition large ongoing force changes are observed in clear contrast to the columnar grain films. In order to illustrate the relation between the film forces and morphological properties TEM micrographs of the Ag film of figure 9 in various growth stages are depicted in figure 10 (from [107]). To reduce restructuring (see subsection 4.1.3) all imaged films were protected with a thin layer of MgF_2 before exposing them to laboratory air. As can be clearly seen, film growth indeed proceeds by Volmer–Weber growth and due to the high

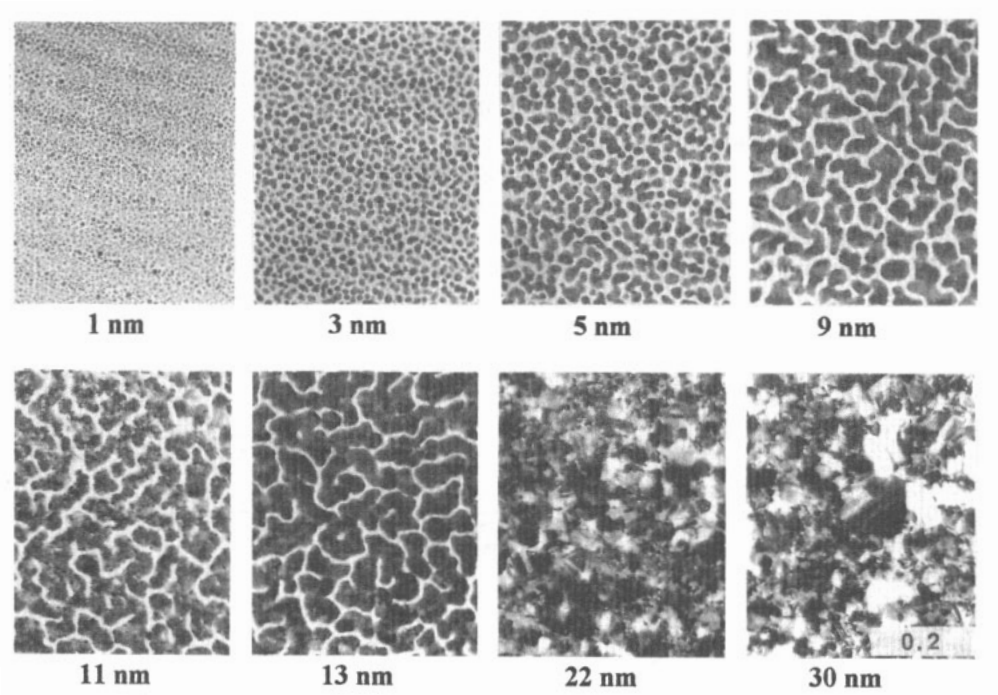

Figure 10. Transmission electron micrographs of Ag films at various mean film thicknesses, UHV deposited at room temperature onto MgF_2 coated glass substrates (from [107]). In order to reduce morphological changes due to recrystallization all films were protected with a thin layer of MgF_2 before exposure to laboratory air. The scale bar is in micrometres.

mobility it is accompanied by lateral grain growth in the continuous film. Initially a large number of nuclei ($\approx 1 \times 10^{16}$ m^{-2}) is formed. Incomplete coalescence to islands with elongated shapes occurs as early as at 2–3 nm; here the first small-angle grain boundaries are formed, which give rise to a respective tensile stress contribution (see subsection 4.1.1). At about 11 nm the Ag film percolates and remains in the channel stage up to about 22 nm, where it becomes completely continuous. On further growth considerable recrystallization leads to a steady increase of the average grain size. Notice that the film thickness t_c at which the film becomes continuous (22 nm) coincides with the film thickness at which the maximum of the force curve appears—a result that has been verified beyond all doubt on many other film/substrate systems (see, e.g., [4] or [108]). Important *in situ* information on the average island radius at percolation R_p can therefore be derived from the thickness value of the force maximum. As illustrated in figure 7, for a growth model [107] consisting of hemispherical islands of uniform size, $R_p = t_c$ when after percolation at first all the channels are filled. Although admittedly the model is based on very crude assumptions, one immediately obtains a rough estimate of the average grain $\overline{D}_c$ size at t_c from the force curves, and thus of the respective island density N_0: $\overline{D}_c = 2R_p = 2t_c$ and $N_0 = (1/\overline{D}_c)^2$. As will be shown in the next two sections, this information is important as it allows us to study the influence of growth conditions on the morphology of thin films by means of *in situ* ISMs. A shift of the force maximum to lower (higher) thickness values points to a decrease (increase) of R_p and correspondingly to an increase (decrease) of N_0.

According to the stress model of Abermann *et al* [10, 12] the film forces in the

discontinuous films (i.e. up to about 22 nm in the case of Ag) are tensile due to the formation of grain boundaries (subsection 4.1.1) and recrystallization (subsection 4.1.3). When the films are continuous, they become compressive due to the dominating effect of the capillarity stress (subsection 4.1.5). Notice, however, that in the continuous films also the measured total film stress is the superposition of the contributions of all three stress mechanisms. The force changes after the film deposition are indicative of ongoing film restructuring (subsection 4.1.3).

From the above growth model one can obtain a rough estimate for the magnitude of the capillarity stress. Inserting the thickness of the force maximum (22 nm) for R_p in equation (6) yields -1.6×10^8 N m^2 for the capillarity stress ($\Phi = 1.8$ N m^{-1} [84]). The total experimental film stress (compressive capillarity stress plus tensile stresses of grain boundaries and recrystallization) determined from the slope of the force curve after the force maximum is -0.7×10^8 N m^2, in reasonable agreement with the calculated value.

5.3. The influence of substrate temperature

As has been discussed in detail in subsection 3.2 the substrate temperature determines the thermal energy of diffusing atoms and is therefore an important external parameter to control film diffusivities. Thurner and Abermann [15] investigated the intrinsic stress of Cr films, which at room temperature grow by columnar grains (subsection 5.1), also at elevated substrate temperatures (figure 11). They found that upon gradually raising the substrate temperature to 570 K the shape of the force curves transforms from that of a low-mobility Volmer–Weber curve to that of a high-mobility Volmer–Weber curve, in agreement with parallel TEM investigations. The average grain size is less than 10 nm at room temperature and about 30 nm at 570 K, the latter value in good agreement with the grain size $\overline{D} = 2t_c$ derived from the respective force curve (≈ 26 nm). An analogous behaviour was observed for the high-melting-point metals Fe [15] and Ti [6].

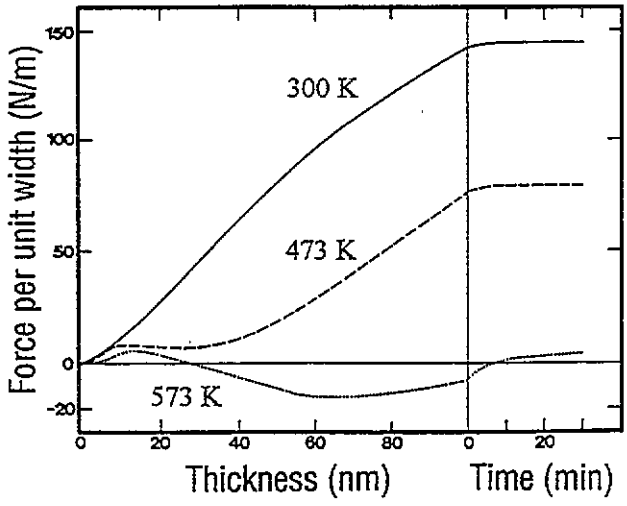

Figure 11. Film forces per unit width against mean thickness (left-hand side) and time (right-hand side) of Cr films UHV deposited at various substrate temperatures onto MgF_2 coated glass substrates: 300 K, 473 K and 573 K (from [15] by courtesy of R Abermann).

Recently it was shown that the growth and stress behaviour of low-melting-point metals is also strongly dependent on the substrate temperature. As depicted in figure 1 (from [17]) the shape of the film forces of polycrystalline Ag UHV deposited onto mica(001) switches from that of a high-mobility Volmer–Weber curve (figure 9) to that of a low-mobility Volmer–Weber curve (figure 8), when the substrate temperature is lowered to 110 K. Similar results were obtained for Cu/mica(110), Au/mica(001) and Ag/MgF_2 [18]. The experiments described in this section therefore convincingly demonstrate that the nature of the intrinsic stress of polycrystalline films is mainly determined by the mobility of the film atoms, which (among other factors) is determined by the material itself and the substrate temperature chosen.

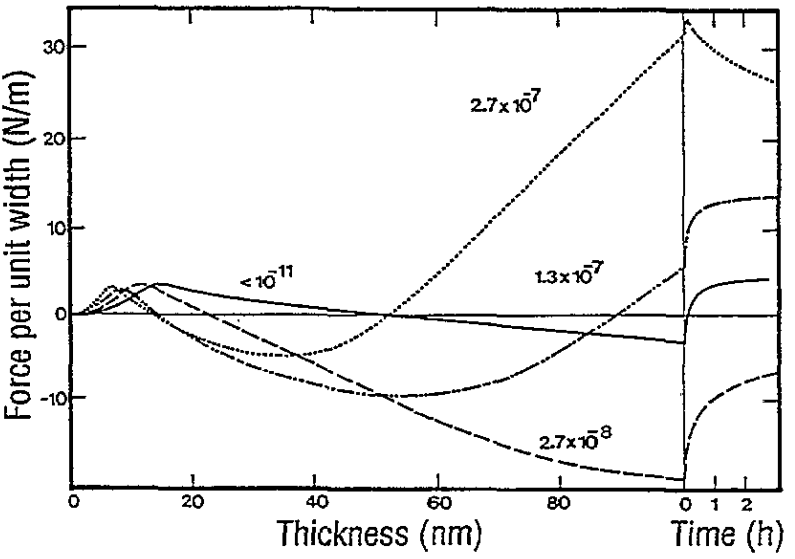

Figure 12. Film forces per unit width against mean thickness (left-hand side) and time (right-hand side) of Cu films UHV deposited at various O_2 partial pressures and 300 K onto MgF_2 coated glass substrates (from [8]); O_2 partial pressures are in millibars.

5.4. The influence of O_2 partial pressure

In the preceding sections it has been shown that growth and stress behaviour of thin films are strongly influenced by the respective mobility of the film material. Here experiments are described where the film mobility is reduced by chemisorbing O on the surface of the growing films. Figure 12 shows the film forces of various Cu films, which were UHV deposited at room temperature onto MgF_2 coated glass substrates (from [8]). The O_2 partial pressure during deposition was raised to 2.7×10^{-7} mbar, which induces a number of striking changes on the film forces: (i) The force maximum is shifted gradually to lower film thicknesses, indicating a reduction of the average island radius R_p at percolation and correspondingly an increase of the island density due to the lower mobility of Cu. (ii) Consequently the compressive slope beyond the force maximum increases, because the capillarity stress depends inversely on R_p (subsection 4.1.5). (iii) Surprisingly at higher film thicknesses the film forces become tensile again as obviously the information of the capillarity strain is lost. This is partially the result of O incorporation into the film and

probably due to a reduced recrystallization rate, which reduces the film's capability to anneal defects. This means that finally—as in the case of the low-mobility Volmer–Weber films—the tensile stress of the grain boundaries (subsection 4.1.1) remains as the dominating stress mechanism.

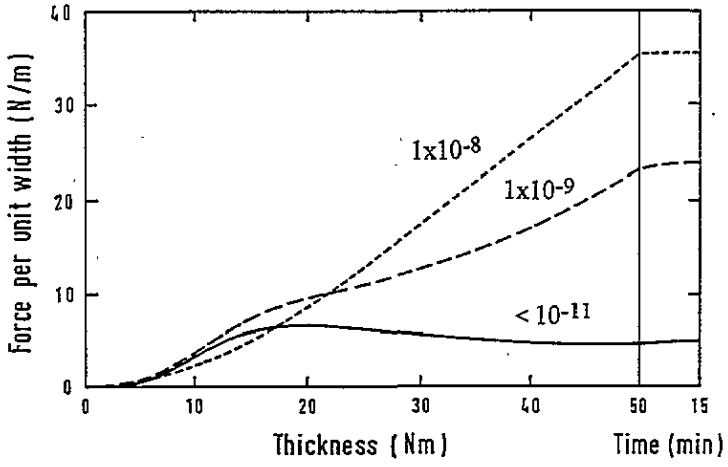

Figure 13. Film forces per unit width against mean thickness (left-hand side) and time (right-hand side) of Ni films UHV deposited at various O_2 partial pressures and 300 K onto MgF_2 coated glass substrates (from [74]); O_2 partial pressures are in millibars.

The Ni/O system (figure 13) provides an example where the O induced transformation to low-mobility Volmer–Weber mode is even more pronounced. The force curve of clean Ni films still reflects high-mobility Volmer–Weber growth, although the lower mobility of Ni compared with Cu is revealed by the vanishing contribution of the capillarity stress. A slight increase of the O_2 partial pressure during deposition to 1.3×10^{-8} mbar ($i^* \approx 10$, subsection 4.1.6) causes the growth and stress behaviour to switch completely to low-mobility Volmer–Weber mode. It should be mentioned that O_2 partial pressures in the 10^{-8}–10^{-9} mbar range are quite common in high-vacuum chambers, so it becomes clear why in previous HV experiments only tensile stresses were measured for Ni films [106, 109].

6. The intrinsic stress of epitaxial thin films

Compared with the large number of investigations performed on polycrystalline thin films only a few deal with the intrinsic stress of epitaxial thin films. This section summarizes the existing results on epitaxial films grown by the three modes of film growth (subsection 3.1): Volmer–Weber, Stranski–Krastanov and Frank–Van der Merwe mode.

6.1. Volmer–Weber epitaxy

It has been well established by many TEM studies that mica(001) constitutes a typical Volmer–Weber substrate for the noble metals Ag, Cu and Au. At elevated substrate temperatures (Ag, 520–570 K [110–112]; Cu, ≈ 670 K [113, 114]; Au, 670 K [111, 115]) film growth proceeds epitaxially with (111) planes parallel to the substrate. In the case of the stress experiments [17, 18] the epitaxial nature of the films was verified with LEED

(figure 14). The respective azimuthal orientations are Ag[11$\bar{2}$], Cu[1$\bar{1}$0] and Au[11$\bar{2}$] parallel mica[100]. Whereas the Ag and Cu films exhibit sharp, single-domain LEED patterns, in the case of Au the degree of epitaxy is less perfect as can be concluded from the faint ring due to randomly oriented (111) facets (not shown in figure 14).

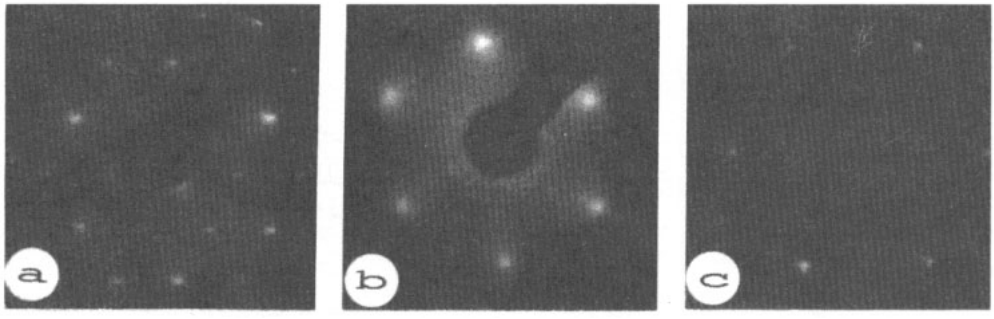

Figure 14. LEED patterns of (a) clean mica(001), primary energy $E_p = 130$ eV, and of 100 nm thick films of (b) Ag, $E_p = 130$ eV, and (c) Cu, $E_p = 130$ eV (from [18]).

As indicated in the introductory section 1 for the Ag/mica(001) system, the transition of film growth from polycrystalline to epitaxial is accompanied by a dramatic change of the intrinsic stress (figure 1). While up to substrate temperatures of about 450 K film forces characteristic of (poycrystalline) high-mobility Volmer–Weber mode are observed (figure 1)—due to the increased mobility the respective force maximum is shifted to higher film thicknesses (see subsection 5.2)—above 450 K large compressive forces appear in the thickness range from 20 nm to 60 nm. The contribution of the compressive force increases with substrate temperature until it saturates at about 570 K. *In situ* conductance measurements revealed that the epitaxial films percolate at film thicknesses at which the respective compressive force arrives at its maximum value ($\approx$ 60 nm for the 570 K film). This means that the appearance of the compressive stress coincides with the network stage of the Ag films and therefore obviously is connected with the formation of domain walls (subsection 4.1.2) being the prevailing growth process of epitaxial Volmer–Weber films close to percolation. As will be discussed in more detail below, in Volmer–Weber epitaxy isolated islands grow with their equilibrium lattice parameter, i.e. free of stress. However, when two islands meet, most likely there is a mismatch at the boundary because each of the islands has nucleated at positions determined by the substrate lattice. The experiments performed so far agree that the strain at 'single-crystalline grain boundaries' is predominantly compressive rather than tensile as in the case of the low-angle grain boundaries of polycrystalline films. At the end of the network stage, part of the compressive strain is released by the sudden formation of misfit dislocations. This interpretation is supported by a previous TEM investigation of Matthews [110], who observed 10^{14}–10^{15} dislocations per square metre in continuous Ag(111) films on mica(001). The tensile stress contribution observed on further film growth and after the film deposition is caused by the recrystallization processes (see below).

Figure 15 collects the intrinsic stress results available so far for epitaxial Volmer–Weber systems: Ag(111) [18] and Cu(111) [18] on mica(001) and Ag(001) on Si(001)(2 $\times$ 1) [19]; the corresponding LEED patterns are depicted in figures 14 and 16. Qualitatively all films are characterized by an analogous dependence of the film forces on film thickness,

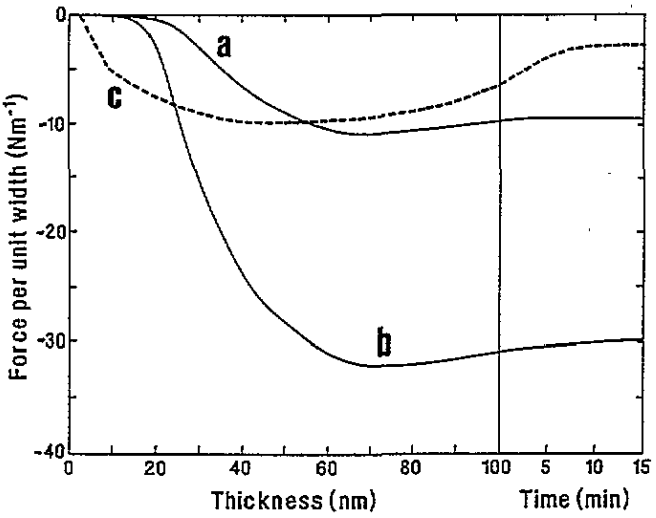

Figure 15. Film forces per unit width against mean film thickness (left) and time (right) of thin metal films growing by epitaxial Volmer–Weber mode: curve a, Ag(111) and curve b, Cu(111) UHV deposited onto mica(001) at 570 K and 715 K, respectively (from [18]); curve c, Ag(001) UHV deposited at 530 K onto p-doped Si(001)(2 × 1) (from [19]).

i.e. in all cases the compressive stress due to domain wall formation dominates the film stress in the respective network stages. STM investigation of the Ag(001) film at a mean thickness of 5 nm impressively demonstrates its epitaxial nature: islands with mainly square and rectangular shapes are imaged (figure 16(c)). Individual islands have lengths between 60 nm and 130 nm and are atomically flat over distances of several tens of nanometres on their upper termination. The many open channels still visible in figure 16(c) confirm the film thickness of 5 nm as lying close to the percolation point of the Ag(001) film. Upon increasing the mean film thickness to 100 nm a remarkable transformation of a film microstructure to an average grain size of about 1 μm has taken place (figure 16(d)), thus, in agreement with the observed tensile stress contribution, indicating considerable recrystallization (subsection 4.1.3). To be fair it should be mentioned that the degree of epitaxial growth on mica(001) is usually subject to some irreproducibility (particularly in the case of Au) due to contaminants always present on air cleaved surfaces [116] and depending on its thermal pretreatment [117]. Nevertheless, for the experiments described above there is always full agreement beween the structural information derived from ISM and LEED, i.e. if the force curves exhibit shapes characteristic of epitaxial growth, sharp LEED patterns are also obtained.

Finally it is interesting to discuss the stress behaviour of Volmer–Weber films during deposition of the first few monolayers. The metal films on mica(001) have grown with orientations causing the smallest the lattice misfit (Ag, 4%; Cu, 2%), which nevertheless would give rise to huge tensile stress in the range of 10^9 N m^{-2} (film forces of 1 N m^{-1} nm^{-1}). In the case of Ag(001)/Si(001)(2 × 1) an epitaxial Ag overlayer with four Ag atoms within three Si lattice spacings constitutes a low-stress surface configuration demanding film forces of 0.3 N m^{-1} nm^{-1}, again a value easily detected with the stress-measuring device. Up to film thicknesses of several monolayers (2–15 nm), however, no film stress is detected at all, indicating that the substrates impose the epitaxial orientation on the growing metal films without transmittance of any lattice misfit. It is noteworthy that

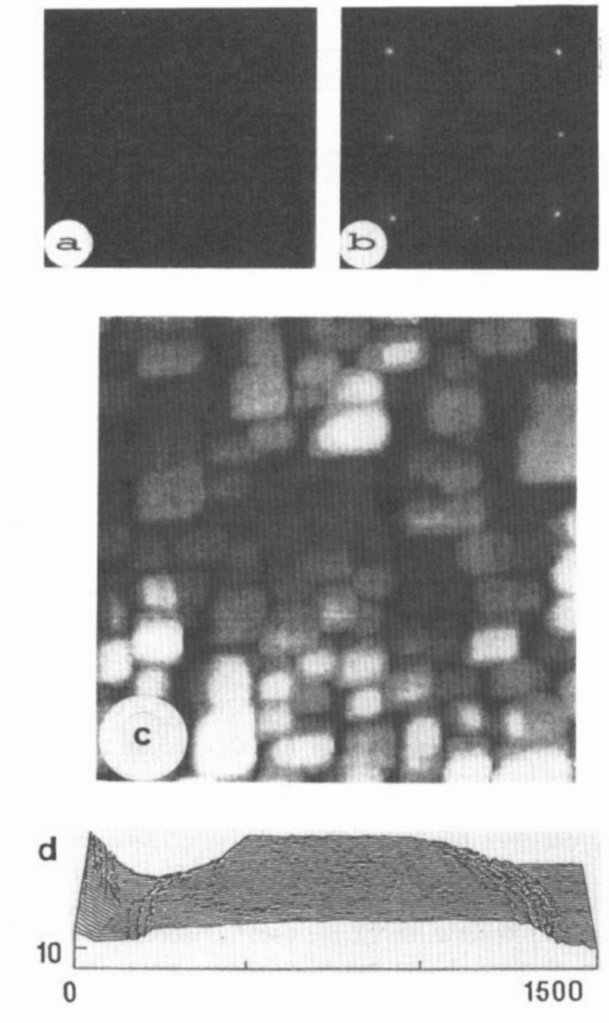

Figure 16. Ag(001)/Si(001)(2 × 1) grown at 530 K by epitaxial Volmer–Weber mode: LEED patterns of (a) Si(001)(2 × 1) and (b) 100 nm thick Ag(001) films, $E_p = 137$ eV. (c) 744 × 744 nm^2 and (d) 1500 × 310 nm^2 STM top view images of 5 nm and 100 nm thick epitaxial Ag(001) films, respectively; $U_t = -500$ mV, $I_t = 10$ nA (from [19]).

Matthews arrived at the same conclusion for the system Ag(111)/mica(001) upon interpreting the Moiré fringes of Ag islands imaged with TEM [90]. The absence of film stress at low film thicknesses is more and more established as a general property of Volmer–Weber growth, for both the epitaxial and polycrystalline versions; this can, however, be easily understood in terms of the limited adhesion due to the weak film/substrate interaction, which is the necessary prerequisite for Volmer–Weber growth (subsection 3.1).

6.2. Stranski–Krastanov epitaxy

The film stress developing during Stranski–Krastanov growth is introduced for Ag(111)/Si(001)(2 × 1), a Stranski–Krastanov system well established in literature. According to a LEED study by Hanbücken and Neddermeyer, flat, epitaxial Ag(111) islands grow at 300 K on top of the Si(001)(2 × 1) dimers [118] without lifting the (2 × 1) reconstruction (figure 17(a)). STM revealed that film growth proceeds by Stranski–Krastanov mode with the initial adsorption of Ag occurring at the twofold bridge sites between adjacent dimer rows [119, 120]. Figure 18 shows the film forces of epitaxial Ag(111) films

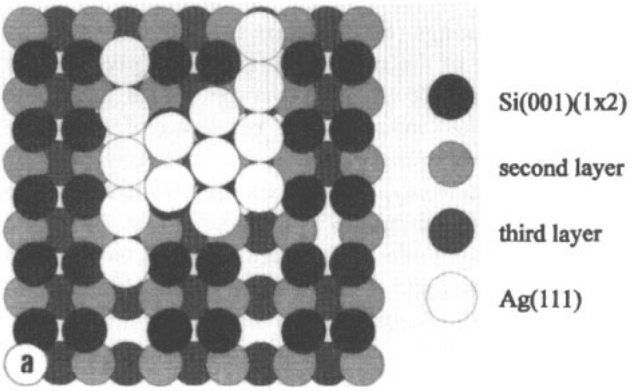

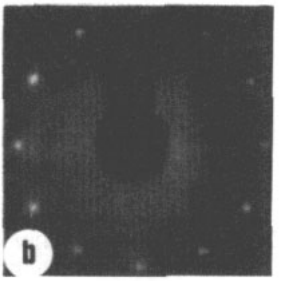

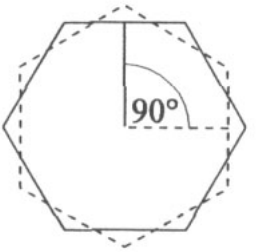

Figure 17. Ag(111)/Si(001)(2 × 1) grown at 300 K by Stranski–Krastanov mode: (a) the structural model according to [118]; (b) the LEED pattern of the two Ag(111) domains, E_p = 134 eV (from [19]).

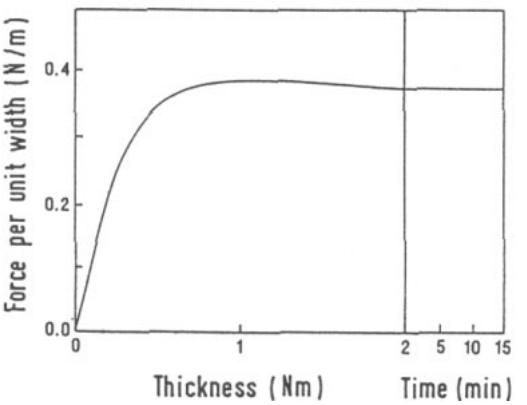

Figure 18. Film forces per unit width against mean film thickness (left) and time (right) of epitaxial Ag(111) films grown at 300 K by Stranski–Krastanov mode on Si(001)(2 × 1) (from [19]).

that—because of the two possible Si(001) terminations—consist of two domains rotated by 90° (compare the LEED pattern of figure 17(b)). In contrast to the epitaxial Volmer–Weber films with neglegible film forces in the initial stages of film growth (subsection 6.1) a huge tensile stress contribution is observed during adsorption of the first three Ag monolayers. The maximum stress of 1.1×10^9 N m^{-2} develops immediately after starting the deposition up to 0.7 monolayers of Ag. The observed stress value is in good agreement with the misfit stress of $(2 \times 10^9)/2$ N m^{-2} calculated for an epitaxial Ag overlayer consisting of three

close-packed Ag rows within two Si lattice spacings (figure 17(a)) as suggested in [118]. The factor of $\frac{1}{2}$ is due to the fact that only one of the two Ag(111) domains gives rise to a bending of the cantilever beam along its long axis. At Ag coverages higher than three monolayers the film forces remain nearly constant indicating the beginning of 3D islanding of the films. The stress results therefore also strongly support the Stranski–Krastanov mode for film growth. Two more points are noteworthy. (i) The good agreement between experimental and calculated misfit stress is really surprising as it suggests that the elastic constants of even ultrathin films are already close to the bulk values. (ii) The misfit strain built up at the interface region of the first monolayers is stored upon further film growth and therefore is not effected by the process of 3D islanding.

Similar results were reported by Schell-Sorokin and Tromp on the semiconductor Stranski–Krastanov system Ge/Si(001)(2 × 1) [21]. The experimental stress of -5.7×10^9 N m^{-2} determined between two and four monolayers of Ge is again in good agreement with the misfit stress of 6.0×10^9 N m^{-2} calculated for a Ge sample compressed by 4.3% as demanded by the lattice mismatch between Si and Ge.

6.3. Frank–Van der Merwe epitaxy

Although layer by layer or Frank–Van der Merwe growth is found frequently for metals growing on metals (see. e.g., [121], [41] or [46]), no results on corresponding film stress have been reported to date. The main reason is certainly the difficulty of preparing metallic single crystals with dimensions of cantilever beam substrates. Recently Winau *et al* [122] investigated the homoepitaxial thin-film system Si/Si(001), where—as should be expected [123]—no film stress is observed; the residual gas pressure during deposition, however, has to be better than 5×10^{-10} mbar. At higher deposition pressures considerable compressive stress develops due to incorporation of gas contaminants into the growing Si films.

Figure 19(a) presents the film forces of epitaxial Fe(001) films UHV deposited onto MgO(001) at 650 K [124]. According to a LEED intensity analysis by Urano and Kanaji [125] film growth proceeds layer by layer with the Fe atoms sitting on top of the O ions at the stage of one monolayer. The film stress of 3×10^9 N m^{-2} corresponding to the linear part of the force curve of figure 19(a) is close to the misfit stress of 6×10^9 N m^{-2}, particularly when considering the lower surface quality of the MgO(001) substrates available compared with the Si substrates. Although the film forces at first sight appear to be similar to those of the Stranski–Krastanov films—huge misfit stress developing during the initial stages of film growth (figure 18)—a remarkable difference becomes evident on closer inspection. In contrast to the Stranski–Krastanov films, where the film forces become constant upon islanding after deposition of a few monolayers (subsection 6.2), in the case of Fe(001)/Mg(001) misfit stress is observed up to 60 monolayers. Obviously then the strain energy is high enough to favour the formation of misfit dislocations as the main mechanism for strain relief on further growth. As in the case of the Stranski–Krastanov films a strained layer is left at the film/substrate interface, which for Fe(001)/Mg(001) has an average thickness of about 8–9 nm. The entire stress behaviour of Fe(001)/Mg(001) therefore also strongly points to Frank–Van der Merwe mode; additional experimental verification by STM is in progress.

7. Conclusions

Systematic investigation of a large variety of thin film systems at different growth conditions performed in the last few years has disclosed many details of the relation between intrinsic

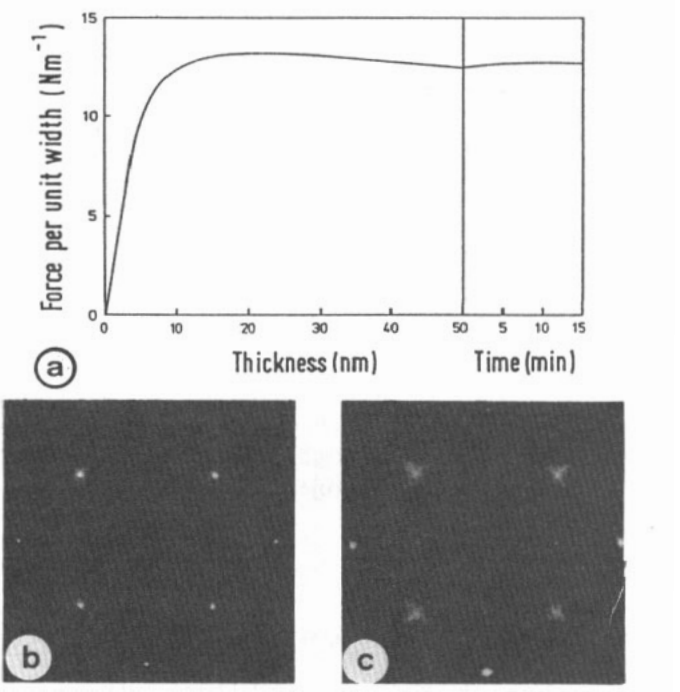

Figure 19. (a) Film forces per unit width against mean film thickness (left) and time (right) of Fe(001) UHV deposited onto MgO(001) at 650 K. (b), (c) LEED patterns of (b) clean MgO(001) and (c) 50 nm Fe(001), $E_p = 93$ eV (from [20]).

stress and the microstructure of the thin films on an atomistic basis. Meanwhile a profound understanding has been achieved for polycrystalline films, where the growth and stress determining parameter was identified in the mobility of the film atoms. Depending on the respective mobilities two different types of film growth are observed, namely low-mobility Volmer–Weber growth (i.e. columnar grain growth) and high-mobility Volmer–Weber growth, both exhibiting quite characteristic stress behaviour. Whereas in low-mobility Volmer–Weber growth the film stress is dominated by the grain boundary stress, in the case of high-mobility Volmer–Weber growth it is the sum of the capillarity, grain boundary and recrystallization stresses. The intrinsic stress of epitaxial thin films has been studied to a much lesser extent. From the results at hand, however, it is already possible to deduce some general aspects, which again point to a growth mode specific stress behaviour that in this case is typical for the three modes of epitaxial growth, i.e. Volmer–Weber, Stranski–Krastanov and Frank–Van der Merwe modes. Perfect homoepitaxial growth basically proceeds free of stress. Both heteroepitaxial Frank–Van der Merwe and Stranski–Krastanov films are generally dominated by large misfit stress in the early stages of film growth, Stranski–Krastanov films during deposition of a few monolayers, Frank–Van der Merwe films up to coverages of several tens of monolayers. The film forces become constant when 3D islands nucleate in Stranski–Krastanov growth, and upon formation of misfit dislocations in Frank–Van der Merwe growth, when the strain energy exceeds a critical value. For the films under investigation a strained layer remains at the film/substrate interface. The Volmer–Weber mode, in contrast, is characterized by the absence of misfit stress during the nucleation and island stages due to the low film/substrate interaction. In the network stage, however, when individual islands coalesce, huge compressive stress

develops upon formation of domain walls because of the mismatch between the islands' nucleation centres. In summary, the experimental results on intrinsic stress and growth of thin films reviewed in this article have led to a very comprehensive picture on the atomistic mechanisms of intrinsic stress, although the general validity of the stress mechanisms involved in epitaxial growth should be tested by other film/substrate combinations. As experimental results clearly show the importance of film stress for film growth phenomena future molecular dynamic studies on the growth of thin films should include the parameter of intrinsic stress.

Acknowledgments

I wish to thank K H Rieder for his permanent scientific and financial support and G Meyer for stimulating discussions and carefully reading the manuscript. The work was partly supported by the Bundesministerium für Forschung und Technologie (Projekt 15N5739) and the Deutsche Forschungsgemeinschaft (Projekt Ko1313).

References

[1] Hoffman R W 1966 *Physics of Thin Films* vol 3, ed G Hass and R E Thun (New York: Academic) p 211
[2] Buckel W 1969 *J. Vac. Sci. Technol.* **6** 606
[3] Campbell D S 1970 *Handbook of Thin Film Technology* ed L I Maissel and R Glang (New York: McGraw-Hill) p 123
[4] Kinosita K 1972 *Thin Solid Films* **12** 17
[5] Kinosita K 1978 *Thin Solid Films* **50** 205
[6] Schneeweiß H J and Abermann R 1992 *Vacuum* **43** 463
[7] Koch R, Leonhard H and Abermann R 1982 *Thin Solid Films* **89** 117
[8] Abermann R and Koch R 1986 *Thin Solid Films* **142** 65
[9] Abermann R 1990 *Thin Solid Films* **186** 233
[10] Abermann R, Koch R and Kramer R 1979 *Thin Solid Films* **58** 365
[11] Abermann R 1990 *Thin Solid Films* **188** 385
[12] Abermann R, Koch R and Martinz H-P 1983 *Vacuum* **33** 871
[13] Klockkolm E and Berry B S 1968 *J. Electrochem. Soc.* **115** 823
[14] Thurner G and Abermann R 1990 *Vacuum* **41** 1300
[15] Thurner G and Abermann R 1990 *Thin Solid Films* **192** 277
[16] Abermann R and Koch R 1985 *Thin Solid Films* **129** 71
[17] Koch R, Winau D, Führmann A and Rieder K H 1991 *Phys. Rev.* B **44** 3369
[18] Winau D, Koch R, Führmann A and Rieder K H 1991 *J. Appl. Phys.* **70** 3081
[19] Koch R, Winau D, Thürmer K, Weber M and Rieder K H 1993 *Europhys. Lett.* **21** 213
[20] Koch R, Winau D and Rieder K H 1993 *Phys. Scr.* T **49** 539
[21] Schell-Sorokin A J and Tromp R M 1990 *Phys. Rev. Lett.* **64** 1030
[22] Martin P J, Netterfield R P, Kinder T J and Stambouli V 1991 *Appl. Phys. Lett.* **58** 2497
[23] Thornton J A and Hoffman D W 1989 *Thin Solid Films* **171** 5
[24] Windischmann H 1991 *J. Vac. Sci. Technol.* A **9** 2431
[25] Murakami M, Angelillo J, Huang H-C W, Segmüller A and Kircher C J 1979 *Thin Solid Films* **60** 1
[26] Ruud J A, Witvrouw A and Spaepen F 1993 *J. Appl. Phys.* **74** 2517
[27] Jona F and Marcus P M 1991 *Surface Physics and Related Topics* ed Fu-Jia Yang *et al* (Singapore: World Scientific) p 213
[28] Stoney G G 1909 *Proc. R. Soc.* A **32** 172
[29] Brenner A and Senderoff S 1949 *J. Res. NBS* **42** 105
[30] Moske M and Samwer S 1989 *Z. Phys.* B **77** 3
[31] Röll K 1976 *J. Appl. Phys.* **47** 3224
[32] Nye J F 1957 *Physical Properties of Crystals* (Oxford: Oxford University Press)
[33] Koch R, Leonhard H, Thurner G and Abermann R 1990 *Rev. Sci. Instrum.* **61** 3859

[34] Sander D and Ibach H 1991 *Phys. Rev.* B **43** 4263
[35] Abermann R and Koch R 1986 *Thin Solid Films* **142** 65
[36] Koch R and Abermann R 1986 *Thin Solid Films* **140** 217
[37] Pashley D W and Stowell M J 1966 *J. Vac. Sci. Technol.* **3** 156
[38] Venables J A, Derrien J and Janssen A P 1980 *Surf. Sci.* **95** 411
[39] Bauer E 1991 *Ber. Bunsenges. Phys. Chem.* **95** 1315
[40] Egelhoff W F Jr and Jacob I 1989 *Phys. Rev. Lett.* **62** 921
[41] Schneider C M, Bressler P, Schuster P, Kirschner J, de Miguel J J and Miranda R 1990 *Phys. Rev. Lett.* **64** 1059
[42] Henzler M 1985 *Quantitative Analysis of* LEED *Spot Profiles (Springer Series in Surface Science 2)* ed M H van Hove and S Y Tong (Berlin: Springer)
[43] Bauer E and Poppa H 1984 *Thin Solid Films* **121** 159
[44] Neddermeyer H 1990 *Crit. Rev. Solid State Mater. Sci.* **16** 309
[45] Lagally M G 1993 *Phys. Today* **46** 24
[46] Kunkel R, Poelsema B, Verheij L K and Comsa G 1990 *Phys. Rev. Lett.* **65** 733
[47] Rosenfeld G, Servaty R, Teichert C, Poelsema B and Comsa G 1993 *Phys. Rev. Lett.* **71** 895
[48] Gilmore C M and Sprague J A 1991 *Phys. Rev.* B **44** 8950
[49] Luedtke W D and Landman U 1991 *Phys. Rev.* B **44** 5970
[50] Kaischew R 1951 *Bull. Acad. Sci. Bulg., Ser. Phys.* **2** 191
[51] Bauer E 1958 *Z. Kristallogr.* **110** 372
[52] Kern R, Le Lay G and Metois J J 1979 *Curr. Top. Mater. Sci.* **3** 131
[53] Yu X, Duxbury P M, Jeffers G and Dubson M A 1991 *Phys. Rev.* B **44** 13 163
[54] Bauer E and van der Merwe J H 1986 *Phys. Rev.* B **33** 3657
[55] Hamers R J, Tromp R M and Demuth J E 1986 *Phys. Rev.* B **34** 5343
[56] Takayanagi K, Tanishiro Y, Takahashi M and Takahashi S 1985 *J. Vac. Sci. Technol.* A **3** 1502
[57] Samsavar A, Hirschorn E S, Miller T, Leibsle F M, Eades J A and Chiang T-C 1990 *Phys. Rev. Lett.* **65** 1607
[58] Brodde A, Badt D, Tosch St and Neddermeyer H 1990 *J. Vac. Sci. Technol.* A **8** 251
[59] Shimaoka G and Komoriya G 1970 *J. Vac. Sci. Technol.* **7** 178
[60] Poelsema B, Kunkel R, Nagel N, Becker A F, Rosenfeld G, Verheij L K and Comsa G 1991 *Appl. Phys.* A **53** 369
[61] Stroscio J A, Pierce D T and Dragoset R A 1993 *Phys. Rev. Lett.* **70** 3615
[62] Burton W K, Cabrera N and Frank F C 1951 *Phil. Trans. R. Soc.* A **243** 299
[63] Ehrlich G and Hudda F G 1966 *J. Chem. Phys.* **44** 1030
[64] Witten T A Jr and Sander L M 1981 *Phys. Rev. Lett.* **47** 1400
[65] Meyer G 1994 private communication
[66] Hwang R Q, Schröder J, Günther C and Behm R J 1991 *Phys. Rev. Lett.* **67** 3279
[67] Röder H, Schuster R, Brune H and Kern K 1993 *Phys. Rev. Lett.* **71** 2086
[68] Nielsen L P, Besenbacher F, Stensgaard I, Lægsgaard E, Engdahl C, Stoltze P, Jacobsen K W and Nørskov J K 1993 *Phys. Rev. Lett.* **71** 754
[69] Egelhoff W F Jr and Steigerwald D A 1989 *J. Vac. Sci. Technol.* A **7** 2167
[70] van der Vegt H A, van Pinxteren H M, Lohmeier M, Vlieg E and Thornton J M C 1992 *Phys. Rev. Lett.* **68** 3335
[71] Wolf D and Lutsko J F 1988 *Phys. Rev. Lett.* **60** 1170
[72] Klockkolm E and Berry B S 1968 *J. Electrochem. Soc.* **115** 823
[73] Abermann R 1990 *Vacuum* **41** 1279
[74] Winau D, Koch R and Rieder K H 1991 *Appl. Phys. Lett.* **59** 1072
[75] Zweck J and Hoffmann H 1984 *J. Magn. Magn. Mater.* **45** 382
[76] Tewes M, Zweck J and Hoffmann H 1991 *J. Magn. Magn. Mater.* **95** 43
[77] Chaudhari P 1972 *J. Vac. Sci. Technol.* **9** 520
[78] Doerner M F and Nix W D 1988 *CRC Crit. Rev. Solid State Mater. Sci.* **14** 225
[79] Mays C W, Vermaak J S and Kuhlmann-Wildorf D 1968 *Surf. Sci.* **12** 134
[80] Moraweck B, Clugnet G and Renouprez A J 1979 *Surf. Sci.* **81** L631
[81] Heyraud J C and Metois J J 1980 *Surf. Sci.* **100** 59
[82] Finegan J D and Hoffman R W 1961 *AEC Technical Report* 18 (Cleveland, OH: Case Institute of Technology)
[83] Thomson W 1958 *Proc. R. Soc.* **9** 255
[84] Sundquist B E 1964 *Acta. Metall.* **12** 67
[85] Macionczyk F, Rohrmann H and Röll K 1994 *Verhandlungen der Deutschen Physikalischen Gesellschaft (DPG-Tagung Münster)* **5** 872

[86] Frank F C and Van der Merwe J H 1949 *Proc. R. Soc.* A **198** 205
[87] Van der Merwe J H 1970 *J. Appl. Phys.* **41** 425
[88] Matthews J W 1975 *Epitaxial Growth* ed J W Matthews (New York: Academic) ch 8
[89] Matthews J W 1975 *J. Vac. Sci. Technol.* **12** 126
[90] Matthews J W 1979 *Dislocations in Solids* vol 2, ed F R N Nabarro (Amsterdam: North-Holland) p 461
[91] Van der Merwe J H and Jesser W A 1988 *J. Appl. Phys.* **64** 4968
[92] Zhang S-L and d'Heurle F M 1992 *Thin Solid Films* **213** 34
[93] Buaud P P, d'Heurle F M, Irene E A, Patnaik B K and Parikh N R 1991 *J. Vac. Sci. Technol.* B **9** 2536
[94] Abermann R 1990 *Thin Solid Films* **188** 385
[95] Winau D, Koch R, Weber M, Rieder K H, Garg R K, Schurig T and Koch H 1992 *Appl. Phys. Lett.* **61** 279
[96] Murakami M 1991 *J. Vac. Sci. Technol.* A **9** 2469
[97] Shuttleworth R1950 *Proc. Phys. Soc.* A **63** 445
[98] Cammarata R C 1994 *Prog. Surf. Sci.* **46** 1
[99] Needs R J 1987 *Phys. Rev. Lett.* **58** 53
[100] Fiorentini V, Methfessel M and Scheffler M 1993 *Phys. Rev. Lett.* **71** 1051
[101] Vanderbilt D 1987 *Phys. Rev. Lett.* **59** 1456
[102] Meade R D and Vanderbilt D 1991 *The Structure of Surfaces III (Springer Series of Surface Science 24)* ed S Y Tong, M A Van Hove, K Takayanagi and X D Xie (Berlin: Springer) p 4
[103] Schell-Sorokin A J and Tromp R M 1990 *Phys. Rev. Lett.* **64** 1030
[104] Sander D and Ibach H 1991 *Phys. Rev.* B **43** 4263
[105] Sander D, Linke U and Ibach H 1992 *Surf. Sci.* **272** 318
[106] Klokholm E and Berry B S 1968 *J. Electrochem. Soc.* **115** 823
[107] Koch R 1981 *Thesis* Universität Innsbruck
[108] Abermann R and Koch R 1980 *Thin Solid Films* **66** 217
[109] Alexander P M and Hoffman R W 1976 *J. Vac. Sci. Technol.* **13** 96
[110] Matthews J W 1962 *Phil. Mag.* **7** 915
[111] Allpress J G and Sanders J V 1967 *Surf. Sci.* **7** 1
[112] Jaeger H, Mercer P D and Sherwood R G 1967 *Surf. Sci.* **6** 309
[113] Stiddard M H B 1982 *Thin Solid Films* **94** 1
[114] Stiddard M H B 1982 *Thin Solid Films* **97** 91
[115] Poppa H, Heinemann K and Elliot A G 1971 *J. Vac.. Sci. Technol.* **8** 471
[116] Poppa H and Elliot A G 1971 *Surf. Sci.* **24** 149
[117] Koch R and Poppa H 1987 *Thin Solid Films* **151** 365
[118] Hanbücken M and Neddermeyer H 1982 *Surf. Sci.* **114** 563
[119] Samsavar A, Hirschorn E S, Leibsle F M and Chiang T C 1989 *Phys. Rev. Lett.* **63** 2830
[120] Brodde A, Badt D, Tosch St and Neddermeyer H 1990 *J. Vac. Sci. Technol.* A **8** 251
[121] Bauer E 1982 *Appl. Surf. Sci.* **11/12** 479
[122] Winau D, Koch R, Weber M, Henze E and Rieder K H to be published
[123] Hamers R J, Köhler U K and Demuth J E 1989 *Ultramicroscopy* **31** 10
[124] Weber M, Winau D, Koch R and Rieder K H to be published
[125] Urano T and Kanaji T 1988 *J. Phys. Soc. Japan* **57** 3403